# Impacts of Aerosols on Seasonal Precipitation and Snowpack in California Based on Convection-Permitting WRF-Chem Simulations

Longtao Wu[1], Yu Gu[2], Jonathan H. Jiang[1], Hui Su[1], Nanpeng Yu[3], Chun Zhao[4], Yun Qian[5], Bin Zhao[2], Kuo-Nan Liou[2], and Yong-Sang Choi[1,6]

[1]*Jet Propulsion Laboratory, California Institute of Technology, Pasadena, CA, USA.*

[2]*Joint Institute for Regional Earth System Science and Engineering and Department of Atmospheric and Oceanic Science, University of California, Los Angeles, CA, USA*

[3]*Department of Electrical and Computer Engineering, University of California, Riverside, Riverside, CA, USA*

[4]*School of Earth and Space Sciences, University of Science and Technology of China, Hefei, Anhui, China*

[5]*Atmospheric Sciences and Global Change Division, Pacific Northwest National Laboratory, Richland, WA, USA*

[6]*Department of Environmental Science and Engineering, Ewha Womans University, Seoul, South Korea*

(Submitted to ACP)

Highlights:

1. Aerosols warm the California mountain tops through aerosol-snow interaction by local dust but cools the lower elevation areas through aerosol-radiation interaction and aerosol-cloud interaction by transported and local anthropogenic aerosols.
2. Aerosols reduce precipitation and snowpack in California primarily through aerosol-cloud interaction by transported and local anthropogenic aerosols and aerosol-snow interaction by local dust.
3. Aerosols cause early snowmelt at mountain tops through aerosol-snow interaction by local dust, and hence modify the seasonal cycle of surface runoff.

**Abstract**

A version of the WRF-Chem model with fully coupled aerosol-meteorology-snowpack is employed to investigate the impacts of various aerosol sources on precipitation and snowpack in California. In particular, the impacts of locally emitted anthropogenic and dust aerosols, and aerosols transported from outside California are studied. We differentiate three pathways of aerosol effects including aerosol-radiation interaction (ARI), aerosol-snow interaction (ASI), and aerosol-cloud interaction (ACI). The convection-permitting model simulations show that precipitation, snow water equivalent (SWE), and surface air temperature averaged over the whole domain (34-42°N, 117-124°W, not including ocean points) are reduced when aerosols are included, therefore reducing large biases of these variables due to the absence of aerosol effects in the model. Aerosols affect California water resources through the warming of mountain tops and the reduction of precipitation; however, different aerosol sources play different roles in changing surface temperature, precipitation and snowpack in California by means of various weights of the three pathways. ARI by all aerosols mainly cools the surface, leading to slightly increased SWE over the mountains. Locally emitted dust aerosols warm the surface of mountain tops through ASI, in which the reduced snow albedo associated with dusty snow leads to more surface absorption of solar radiation and reduced SWE. Transported aerosols and local anthropogenic aerosols play a dominant role in increasing non-precipitating clouds but reducing precipitation through ACI, leading to reduced SWE and runoff over the Sierra Nevada, as well as the warming of mountain tops associated with decreased SWE and hence lower surface albedo. The average changes in surface temperature from October 2012 to June 2013 are about –0.19 K and 0.22 K for the whole domain and over mountain tops, respectively. Overall, the averaged reduction during October to June is about 7% for precipitation, 3% for SWE, and 7% for surface runoff for the whole domain,

while the corresponding numbers are 12%, 10%, and 10% for the mountain tops. The reduction in SWE is more significant in a dry year, with 9% for the whole domain and 16% for the mountain tops. The maximum reduction of ~20% in precipitation occurs in May associated with the maximum of aerosol loadings, leading to the largest decrease in SWE and surface runoff over that period. It is also found that dust aerosols could cause early snowmelt at the mountain tops and reduced surface runoff after April.

## 1. Introduction

Water resources in California are derived predominantly from precipitation (mostly during the winter time) and storage in the snowpack in the Sierra Nevada. Snowpack provides about one-third of the water used by California's cities and farms. The fresh water stored in the snowpack gradually releases through runoff into river flows during the warm and dry season. The amount and timing of snowmelt are critical factors in determining water resources in this region. It is important to understand the factors influencing precipitation and snowpack on seasonal timescale for water management and hydropower operation.

The 2012-2014 California drought has been attributed to both warming and anomalously low precipitation (Griffin and Anchukaitis, 2014). Previous studies suggested that warming trends are amplified in mountains compared to lowlands (Pepin et al., 2015). The amplified warming in mountain areas, also referred to as elevation-dependent warming, is generally attributed to a few important processes (Pepin et al., 2015), such as water vapor changes and latent heat release, surface water vapor changes, radiative flux changes associated with three-dimensional rugged topography (Gu et al., 2012a; Liou et al., 2013; Lee et al., 2015; Zhao et al., 2016), and snow-

albedo feedback (Leung et al., 2004). A review and assessment of the mechanisms contributing to an enhanced warming over mountain areas is given in Pepin et al. (2015).

In addition to the warming effects of greenhouse gases, aerosols may have substantial impacts on water resources in California. Recent observational and numerical modeling studies have shown that aerosol pollutants can substantially change precipitation and snowpack in California (e.g., Rosenfeld et al., 2008a; Qian et al., 2009a; Hadley et al., 2010; Ault et al., 2011; Creamean et al., 2013, 2015; Fan et al., 2014; Oaida et al., 2015). Lee and Liou (2012) illustrated that approximately 26% of snow albedo reduction from March to April over the Sierra Nevada is caused by an increase in aerosol optical depth (AOD).

In California, aerosols can be generated locally or transported from remote sources. Among local aerosol types, dust comprises a significant fraction over California (Wu et al., 2017). Based on a four-month, high intensity record of size-segregated particulate matter (PM) samples collected from a high elevation site, Vicars and Sickman (2011) found that the mass concentration of coarse atmospheric PM in the southern Sierra Nevada, California, was dominated by contribution from dust (50-80%) throughout the study period. Dust aerosols can exert important impact on radiative forcing and regional climate in California through its interaction with radiation (e.g., Zhao et al., 2013a) as well as its role as cloud condensations nuclei for cloud formation (e.g., Fan et al., 2014). Anthropogenic aerosols are geographically distributed because of localized emission sources, the short atmospheric residence time, and regional topography. With valleys and surround mountain barriers, dispersion of air pollutants is more difficult for locally emitted anthropogenic air pollution. The anthropogenic aerosols can cause changes in atmospheric circulation and regional climate especially where the aerosol concentrations are high and the synoptic atmospheric systems

are not prominent (e.g., Qian et al., 2003; Fast et al., 2006; Rosenfeld et al., 2008a; Zhao et al., 2013a).

Besides the local aerosol sources, the atmospheric transport of aerosol pollutants from the Asian continent (e.g., Jiang et al., 2007; Wang et al., 2015; Hu et al., 2016) is also a significant contributor to aerosol loading throughout the Pacific basin. Asian aerosols can reach relatively high concentrations above the marine boundary layer in the western US, representing as much as 85% of the total atmospheric burden of PM at some sites (VanCuren, 2003). Trans-Pacific dust transport has been found to be particularly relevant in high-elevation regions such as the Sierra Nevada, which typically represents free-tropospheric conditions due to the limited transport of lowland air pollutants and predominance of upper air subsidence (VanCuren et al., 2005). Observations from the CalWater campaign demonstrated that dust and biological aerosols transported from northern Asia and the Sahara were present in glaciated high-altitude clouds in the Sierra Nevada coincident with elevated ice nuclei (IN) particle concentrations and ice-induced precipitation (Ault et al., 2011; Creamean et al., 2013).

Aerosols can influence precipitation, snowpack and regional climate through three pathways: (1) aerosol-radiation interaction (ARI, also known as aerosol direct effect), which can warm the atmosphere but cool the surface, resulting in changes in thermodynamic environment for cloud and precipitation and the delay of the snowmelt (Charlson et al., 1992; Kiehl and Briegleb, 1993; Hansen et al., 1997; Koren et al., 2004; Gu et al., 2006, 2016, 2017); (2) aerosol-cloud interaction (ACI, also known as aerosol indirect effect), which is related to aerosols serving as cloud condensation nuclei (CCN) and IN. By changing the size distribution of cloud droplets and ice particles, aerosol may affect cloud microphysics, radiative properties and precipitation efficiency, thus affect the atmospheric hydrological cycle and energy balance (Twomey, 1977; Jiang and

Feingold, 2006; Rosenfeld et al., 2008b; Qian et al., 2009b; Gu et al., 2012b); (3) aerosol-snow interaction (ASI). When aerosols (mainly absorbing aerosols, such as dust and black carbon) are deposited on snowpack, they can reduce snow albedo and affect snowmelt (Warren and Wiscombe, 1985; Jacobson, 2004; Flanner et al., 2007; Qian et al., 2011, 2015; Zhao et al., 2014). Numerical experiments have shown that ARI reduces the surface downward radiation fluxes, cools the surface and warms the atmosphere over California (Kim et al., 2006; Zhao et al., 2013a), which could subsequently impact clouds, precipitation and snowpack. In a 2-D simulation, Lynn et al. (2007) shows that ACI decreases orographic precipitation by 30% over the length of the mountain slope. Fan et al. (2014) showed that ACI increases the accumulated precipitation of an Atmospheric River event by 10-20% from the Central Valley to the Sierra Nevada due to a ~40% increase in snow formation. Snow impurities (ASI) increase ground temperature, decrease snow water, shorten snow duration and cause earlier runoff (Jacobson, 2004; Painter et al., 2007, 2010; Qian et al., 2009a; Waliser et al., 2011; Oaida et al., 2015).

Although recent studies showed that aerosols can substantially influence precipitation and snowpack in California, they focused only on one of the aerosol sources or on a single event or one pathway. A complete account of the aerosol impacts from different sources through three pathways on regional climate in California has not been presented yet. The objective of this study is to investigate the impacts of various aerosol sources on seasonal precipitation and snowpack in California. A fully coupled high-resolution aerosol-meteorology-snowpack model will be used. We will distinguish and quantify the impacts of aerosols from local emissions and transport, and the roles of different prevailing aerosol types in California, particularly dust and anthropogenic aerosols. In Section 2, we describe the WRF-Chem model employed and experiments designed to

142 understand the impact of aerosols on precipitation and snowpack in California. Results from model
143 simulations are discussed in Section 3. Concluding remarks are given in Section 4.
144
145 **2. Model Description and Experiment Design**
146 This study uses a version of the Weather Research and Forecasting (WRF) model with
147 chemistry (WRF-Chem; Grell et al., 2005) improved by the University of Science and Technology
148 of China (USTC) based on the public-released version 3.5.1 (Zhao et al., 2014). ASI is
149 implemented in this WRF-Chem version by considering aerosol deposition on snowpack and the
150 subsequent radiative impacts through the SNow, ICe, and Aerosol Radiative (SNICAR) model
151 (Zhao et al., 2014). The SNICAR model is a multilayer model that accounts for vertically
152 heterogeneous snow properties and heating and influence of the ground underlying snow (Flanner
153 and Zender, 2005; Flanner et al., 2007, 2009, 2012). The SNICAR model uses the theory from
154 Wiscombe and Warren (1980) and the two-stream, multilayer radiative approximation of Toon et
155 al. (1989). SNICAR simulates snow surface albedo as well as the radiative absorption within each
156 snow layer. It can also simulate aerosol content and radiative effect in snow, and was first used to
157 study the aerosol heating and snow aging in a global climate model by Flanner et al. (2007).
158 Simulated change of snow albedo by SNICAR for a given black carbon concentration in snow has
159 been validated with recent laboratory and field measurements (Brandt et al., 2011; Hadley and
160 Kirchstetter, 2012). More detailed description of the SNICAR model can be found in Flanner and
161 Zender (2005) and Flanner et al. (2007, 2012).
162 The MOSAIC (Model for Simulating Aerosol Interactions and Chemistry) aerosol model
163 (Zaveri et al., 2008) with the CBM-Z (carbon bond mechanism) photochemical mechanism (Zaveri
164 and Peters, 1999) is used and coupled with the SNICAR model. The MOSAIC aerosol scheme

uses the sectional approach to represent aerosol size distributions with a number of discrete size bins, either four or eight bins in the current version of WRF-Chem (Fast et al., 2006). In this study, aerosol particles are partitioned into four-sectional bins with dry diameter within 0.039-0.156 μm, 0.156-0.625 μm, 0.625-2.5 μm, and 2.5-10.0 μm. The 4-bin approach has been examined in dust simulations and proved to reasonably produce dust mass loading and AOD compared with the 8-bin approach (Zhao et al., 2013b). All major aerosol components including sulfate, nitrate, ammonium, black carbon, organic matter, sea salt, and mineral dust are simulated in the model. The MOSAIC aerosol scheme includes physical and chemical processes of nucleation, condensation, coagulation, aqueous phase chemistry, and water uptake by aerosols. Dry deposition of aerosol mass and number is simulated following the approach of Binkowski and Shankar (1995), which includes both particle diffusion and gravitational effects. Wet removal of aerosols by grid resolved stratiform clouds/precipitation includes in-cloud removal (rainout) and below-cloud removal (washout) by impaction and interception, following Easter et al. (2004) and Chapman et al. (2009). In this study, cloud-ice-borne aerosols are not explicitly treated in the model but the removal of aerosols by the droplet freezing process is considered. Aerosol optical properties such as extinction, single scattering albedo (SSA), and asymmetry factor for scattering are computed as a function of wavelength for each model grid box. Aerosols are assumed internally mixed in each bin, i.e., a complex refractive index is calculated by volume averaging for each bin for each chemical constituent of aerosols (Barnard et al., 2010; Zhao et al., 2013a). The Optical Properties of Aerosols and Clouds (OPAC) data set (Hess et al., 1998) is used for the shortwave (SW) and longwave (LW) refractive indices of aerosols, except that a constant value of 1.53+0.003i is used for the SW refractive index of dust following Zhao et al. (2010, 2011). A detailed description of

187 the computation of aerosol optical properties in WRF-Chem can be found in Fast et al. (2006) and
188 Barnard et al. (2010).

189 ARI is included in the radiation scheme as implemented by Zhao et al. (2011). The optical
190 properties and direct radiative forcing of individual aerosol species in the atmosphere are
191 diagnosed following the methodology described in Zhao et al. (2013a). The activation and re-
192 suspension between dry aerosols and cloud droplets are included in the model as shown in
193 Gustafson et al. (2007). By linking simulated cloud droplet number with shortwave radiation and
194 microphysics schemes, ACI is effectively simulated in the model (Chapman et al., 2009).

195 The model setups (Table 1), including the physical schemes used, follow Wu et al. (2017),
196 which showed that the model simulations reasonably captured the distribution and variation of
197 aerosols in the San Joaquin Valley. The model domain covers the Western US centered at 38°N
198 and 121°W, as shown in Fig. 1. The horizontal resolution is 4 km × 4 km together with a vertical
199 resolution of 40 model levels. Model integrations with a time step of 20 seconds have been
200 performed for 10 months (with the first month used for the model spin-up) starting on September
201 1, 2012, at 00:00UTC till the end of June 2013 to cover the major precipitation and snow seasons.
202 To test the robustness of the results, simulations are also conducted for year 2013-2014, and similar
203 results are found. In the following section, our analysis focuses on year 2012-2013, while
204 quantitative information of the aerosol impacts for year 2013-2014 is provided for comparison.

205 Note that convective processes are resolved in the 4 km simulations. One important subgrid
206 process in climate models is the representation of deep convection. Parameterizing deep
207 convection is challenging and the use of convection parameterization schemes leads to common
208 errors such as misrepresentation of the diurnal cycle of convective precipitation (e.g., Dai et al.,
209 1999; Brockhaus et al., 2008), underestimation of dry days (e.g., Bergetal., 2013) and precipitation

intensity (e.g., Prein et al., 2013; Fosser et al., 2014; Ban et al., 2014), and overestimation of low-precipitation frequency (e.g., Bergetal., 2013). Although recently developed parameterization schemes lead to improvements in the simulation of precipitation intensity (Donner et al., 2011), intraseasonal variability (Benedict et al., 2013), and diurnal cycles (Bechtold et al., 2014), a promising remedy to the error-prone model simulations using convective parameterizations is the use of convection-permitting horizontal resolution with grid spacing of about 4 km or less (e.g., Satoh et al., 2008; Prein et al., 2013; Ban et al., 2014). Advances in high-performance computing allowed refinement of the model grids well below 10 km. At these scales, convection parameterization schemes may be switched off as deep convection starts to be resolved explicitly (e.g., Weisman et al., 1997). According to Prein et al. (2014), it seems prudent to use horizontal grid spacing of 4 km or less for convection-permitting model simulations. The 4 km simulation can also represent topography and inhomogeneous distribution of anthropogenic emission and precipitation better, leading to a better representation of aerosol distribution comparing to the 20 km simulation (Wu et al., 2017).

Since the model explicitly considers different sources and types of aerosols and contains the physical processes to represent various aerosol effects (ARI, ASI, and ACI), it is useful to decompose the aerosol effects based on aerosol sources/types and pathways. Note that the overall aerosols effects are not a simple sum of different aerosol sources/types, nor a linear combination of the ARI, ASI, and ACI effects. Differences between various simulations, however, help to identify the effect of a single source or pathway and the decomposition approach is a common practice in the experiment design of modeling studies. To examine the overall aerosol effects and the roles of locally generated and transported aerosols, the following five experiments have been designed (Table 2):

1) CTRL: This is the control experiment with all aerosol emissions and transports included in the simulation.

2) NoLocDust: This experiment is performed without any local dust emission. Differences between the CTRL and NoLocDust experiments illustrate the effect of dust aerosols locally emitted.

3) NoLocAnth: This experiment is similar to NoLocDust, except that emissions of local anthropogenic aerosols are turned off. Comparison between CTRL and this experiment will elucidate the effect of local anthropogenic aerosols.

4) NoTran: The initial and boundary chemical conditions in the CTRL simulation are taken from the global Model for Ozone and Related Chemical Tracers, version 4 (MOZART-4; Emmons et al., 2010). The chemical species transported into the model domain include organic carbon, black carbon, sulfate, nitrate, ammonium, sea salt, dust, etc.. In the NoTran experiment, aerosols transport from outside the model domain, including those from East Asia and other regions, are not considered by setting the lateral boundary conditions for aerosols to zero. Differences between CTRL and NoTran will show the effect of transported aerosols.

5) CLEAN: This experiment is performed without any local aerosol emissions or transport from outside the model domain while all the transported chemical species are kept, and therefore represents a scenario of clean condition. Aerosols are low in the simulation, but not zero, possibly due to aerosol chemistry. The CCN concentration at supersaturation of 0.1% is on the order of 10 $cm^{-3}$ at most time of the CLEAN simulation. The distribution of liquid water path and ice water path in the CLEAN simulation is also similar to that in the CTRL simulation, with differences in magnitude. Differences between the CTRL and CLEAN experiments would illustrate the effects

of all primary aerosol types, including those locally emitted and transported from outside the domain.

In order to distinguish the pathways through which the aerosols influence the precipitation and snowpack, we also conducted a few other experiments (Table 3):

6) NARI: This experiment is similar to the CTRL run, except that ARI is not included. Comparison between CTRL and this experiment will elucidate the effect of ARI.

7) NASI: This experiment is similar to the CTRL run, except that ASI is not included. Comparison between CTRL and this experiment will show the effect of ASI.

8) NARS: This experiment is similar to the CTRL run, except that both ARI and ASI are not included. By comparing this experiment and CLEAN, the effect due to ACI can be examined.

## 3. Model Simulation Results

### 3.1 Validation of Model Results

Since our focus is on the changes in precipitation and snowpack due to aerosol effects, we first show the spatial distribution of averaged results over the period from October 2012 to June 2013 when snow normally presents over the Sierra Nevada. Figure 2 illustrates a few important and relevant variables that the model simulates in the CTRL experiment, including liquid water path (LWP), ice water path (IWP), precipitation, snow water equivalent (SWE), and temperature at two meters (T2) above the ground. SWE is a common snowpack measurement. It is the amount of water contained within the snowpack and can be regarded as the depth of water over unit flat surface that would theoretically result if the entire snowpack melted instantaneously. Here, the model simulated SWE is the mean value of the accumulated SWE from 3-hourly model outputs. It is shown that clouds (Fig. 2a and 2b), precipitation (Fig. 2c), snowpack (Fig. 2d), and surface

runoff (Fig. S1) mostly occur over the Sierra Nevada and Klamath Mountains in northern California. For temperature (Fig. 2e), the central valley area appears to be relatively warm with two maxima over the northern and southern part of the central valley, respectively, while colder temperatures are found over the mountain ranges. The model-simulated precipitation is compared with corresponding observations from the Parameter elevation Regression on Independent Slopes Model (PRISM, 2004) gridded data product at 4 km resolution (Fig. 2f). Note that the precipitation rate in comparison here is for total precipitation, including rainfall and ice-phase particles. Compared to the PRISM observations, the model successfully captures the precipitation pattern, including the locations of the major precipitation centers, but slightly overestimates the magnitude over the Sierra Nevada.

In order to validate the simulated seasonal variations, the monthly mean model simulated precipitation and T2 are compared with observations (Fig. 3a and 3c). Model data are sampled onto observational sites before the comparison is conducted. For precipitation observations, besides the PRISM product, we also employ the Climate Prediction Center (CPC) Unified Gauge-Based Analysis of Daily Precipitation product (Chen et al., 2008) at $0.25° \times 0.25°$ resolution and the gauge measurements from Department of Water Resources (DWR). Observed air temperature is obtained from the California Irrigation Management Information System (Snyder, 1984). For SWE, daily accumulated SWE simulations are compared with measurements collected at Snow Telemetry (SNOTEL) stations. SNOTEL SWE is measured using a snow pillow sensor and biases in SWE measurement could occur when temperature differences between surrounding ground cover and the pillow sensor create uneven distribution of snow (Meyer et al., 2012). Both under- and over-estimation could happen depending on the snowmelt conditions and the snow density rate of change (Serreze et al., 1999; Serreze et al., 2001; Johnson and Marks, 2004).

It is shown that the model captures the maximum precipitation in December, with the magnitude falling between the observations from CPC and PRISM/DWR during winter, which is the major rainy season in California (Fig. 3a). In the relative dry months from February to June, the simulated precipitation has similar magnitude to the observations, with slightly overestimation or underestimation in different months. For SWE, the model simulations represent seasonal variations of SWE with the maximum between March and April (Fig. 3b), but the model overestimates SWE amount comparing to SNOTEL. While the model overestimates the surface temperature in magnitude, it captures the seasonal variations well, including the highest/lowest temperature in July/January, respectively (Fig. 3c).

The simulated aerosols over California using this model have been validated extensively in Wu et al. (2017) by comparing to observations, such as MISR (Multiangle Imaging Spectroradiometer) and AERONET (Aerosol Robotic Network) AOD, CALIPSO (Cloud-Aerosol Lidar and Infrared pathfinder Satellite Observation) aerosol extinction, IMPROVE (Interagency Monitoring of Protected Visual Environments) and EPA CSN (National Chemical Speciation Network operated by Environmental Protection Agency) aerosol speciation. It has been shown than the model simulation used in this study reasonably captures the distribution and seasonal variation in aerosols during the cold season from October to March. The simulation of aerosols in the warm season from April to September (especially from July to September) has larger low biases than in the cold season, mainly due to poor simulations of dust emission and vertical mixing. Because the precipitation and snow mainly occur in October-June, we focus on the simulations from October to June with relative good performance on aerosol simulations in this study.

Here, we present the distributions of AOD averaged over October 2012 to June 2013 for the MISR (Diner et al., 1998) observation and all aerosols in the CTRL simulation, together with

locally emitted aerosols and those transported from outside the model domain, derived from the difference between the CTRL simulation and the corresponding experiment (NoLocAnth, NoLocDust and NoTran), respectively, to facilitate the understanding of the aerosol effects in different regions and from different sources (Fig. 4). It is shown that the model simulation well captures the spatial distribution of AOD in California, including the maximum over the southern part of the valley area and larger AODs over the lower lands to the southeast of the Sierra Nevada (Fig. 4a and 4b). Note that the smoother contour in MISR is due to the coarser horizontal resolution (0.5°) of the MISR data. The distribution of the locally emitted anthropogenic aerosols (Fig. 4c), which are mostly located over the central valley associated with the emissions from local industries and farms, presents a similar pattern to the total AOD and substantially contributes to the maxima AOD over the region. Local dust aerosols mainly reside over the lower lands to the southeast of the Sierra Nevada while substantial amounts are also seen over the central valley (Fig. 4d). Transported aerosols are carried into the domain by atmospheric circulation and widely distributed, with more over the central valley due to the trapping of aerosols by the surrounding mountains (Fig. 4e).

Since the observations on aerosol-in-snow concentrations are rather limited both spatially and temporally, it's very difficult to conduct direct comparisons with model simulations. Here we evaluate the model simulations of snow albedo which is directly affected by the ASI (Fig. S2). The model simulated snow albedo is compared with the product from NASA Land Data Assimilation Systems (NLDAS; Sheffield et al., 2003) Mosaic (MOS). It is shown that model simulation provides rather reasonable estimate of the snow albedo when ASI is included. Overall, the WRF-Chem model that we employ in this study is a reliable tool for examining the impact of aerosols

346 on the seasonal variations of precipitation and snowpack in California, especially over the Sierra
347 Nevada.
348
349 **3.2 Aerosol Effects on Precipitation and Snowpack**
350 The overall aerosol effects, from all aerosol types and sources (including locally emitted and
351 transported) through the three pathways (ARI, ASI, and ACI), can be examined from the
352 differences between the experiments CTRL and CLEAN. The two-tailed Student's t test, in which
353 deviations of the estimated parameter in either direction are considered theoretically possible, is
354 applied to the 3-hourly data for each experiment in this study to measure the statistical significance
355 of the simulations. Figure 5 shows the differences averaged over October 2012 to June 2013 in
356 precipitation, SWE, and T2, where the dots represent differences of the 3-hourly data being
357 statistically significant at above 90% level. Due to the aerosol effects, temperature decreases over
358 the central valley, where most aerosols are located, while significant warming occurs over the
359 mountain tops (Fig. 5c). Precipitation decreases over the Sierra Nevada (Fig. 5a), consequently
360 leading to decreased SWE (Fig. 5b).
361 In order to understand how the aerosols affect these important variables, we examine the
362 effects of ARI, ASI, and ACI separately. In the following figures (Fig. 6 to Fig. 12), the differences
363 are statistically significant at 70% level. It is seen that the major effect of ARI is to decrease the
364 surface temperature over the whole domain through the scattering and absorption of solar radiation,
365 with the maxima over the central valley where the aerosols are mostly located, contributing to the
366 surface cooling caused by the total aerosols effects in that region (Fig. 6c). The ARI induced
367 surface cooling over the Sierra Nevada, although not as strong as over the central valley, leads to
368 reduced snowmelt and hence slight increase in SWE, opposite to the overall aerosol effect on SWE

(Fig. 6b). The effect of ARI on rainfall is not very significant (Fig. 6a). The main effect of ASI is to increase the temperature (Fig. 7c) over the snowy area of the Sierra Nevada through the reduction of snow albedo (Fig. 7d) and hence more absorption of solar radiation at the surface, contributing to the reduced SWE over the Sierra Nevada (Fig. 7b). The effect of ASI on precipitation is also minimal.

Figure 8 shows the effect of aerosols on clouds through ACI. When more aerosols are present in the atmosphere, more CCN are available for the formation of clouds with smaller cloud droplets. As a result, more non-precipitating clouds are produced when aerosol are included in the model. The enhanced LWP (Fig. 8a) is primarily produced by the ACI effect (Fig. 8c). There are no significant changes in IWP (including ice, snow, and graupel) because the aerosol effect on ice cloud formation is not explicitly treated in the model. The ACI effect leads to reduced precipitation and less SWE over the mountains (Figs. 9a and 9b). Temperature decreases over the valley due to more clouds formed associated with the ACI effect. The increase in temperature over the mountain areas (Fig. 9c) is caused by the reduced snow amount, which results in weaker surface albedo (Fig. 9d) and enhanced solar absorption at the surface and overwhelms the decrease of temperature which may be caused by increased clouds.

Overall, aerosols affect surface temperature, precipitation, and snowpack in California through the three pathways. ACI plays a dominant role in increasing cloud water but reducing precipitation, leading to reduced SWE and surface runoff (Fig. S3) over the Sierra Nevada. ASI also reduces SWE due to the smaller snow albedo associated with dirty snow, leading to more surface absorption and snowmelt. ARI, on the other hand, slightly increases SWE through the cooling of the surface. For surface temperature, ARI and ACI contribute together to the cooling of the valley area, while ACI and ASI significantly warm the surface over the mountain tops. Note

that for the ASI effect, warming of the snow cover area through aerosol induced snow-albedo feedback is the cause for the reduced SWE. For the ACI effect, however, warming over the mountain region is a result from the reduced SWE which can also induce snow-albedo feedback and result in smaller surface albedo and more surface absorption of solar radiation.

Next, we examine the roles of local anthropogenic aerosols and local dust as well as transported aerosols. The effect of local anthropogenic aerosols can be discovered from the differences between CTRL and NoLocAnth. It is shown that local anthropogenic aerosols slightly suppress precipitation (Fig. 10a) via ACI, leading to a reduced SWE (Fig. 10b) and a warming over the mountain tops (Fig. 10c). The cooling of the valley area, where locally emitted anthropogenic aerosols are mostly located (Fig. 4b), is associated with both the ARI effect and more non-precipitating clouds produced through ACI. Dust aerosols emitted from local sources mainly warm the surface through the reduction of snow albedo (ASI, Fig. 11c), consequently enhancing the snowmelt and leading to the reduced SWE (Fig. 11b). Local dust aerosols have no significant effect on precipitation (Fig. 11a).

Note that the effects of local anthropogenic and dust aerosols do not seem to be able to explain the total effects of aerosols as seen in Fig. 5, raising the question whether the transported aerosols play an important role in the precipitation and snowpack over the Sierra Nevada. Figure 12 illustrates the impact of aerosols transported from outside the model domain. It is shown that transported aerosols reduce the precipitation through ACI (Fig. 12a), which exceeds the ARI effect and leads to decreased SWE and increased temperature over the southern part of the Sierra Nevada (Fig. 12b and 12c). Over the central valley, as well as over the northern part of the Sierra Nevada, temperature decreases (Fig. 12c) due to the relatively larger ARI effect of the transported aerosols

414 compared to the ACI effect, resulting in less snowmelt and increased SWE over that region (Fig.
415 12b).

416 The overall changes induced by aerosols for surface temperature (K) and precipitation, SWE,
417 and surface runoff in percentage averaged over October to June are given in Table 4 for the whole
418 domain (34-42 °N, 117-124 °W, not including ocean points), mountain tops (elevation ≥ 2.5 km),
419 and lower elevations (elevation < 2.5 km). For the whole domain in year 2012-2013, temperature
420 is cooled by 0.19 K due to aerosol ARI (–0.14 K), as well as ACI (–0.06 K) mainly associated
421 with transported aerosols (–0.17 K), accompanied by reduction in precipitation, SWE, and surface
422 runoff of about 7%, 3%, and 7%, respectively. Reduction in precipitation is mainly caused by ACI
423 (–6.26%) associated with transported (–2.97%) and local anthropogenic (–1.02%) aerosols. For
424 SWE, reduction is attributed to ACI (–2.67%) and ASI (–1.96%), while ARI contributes to an
425 increase (1.88%). Surface runoff is defined as water from precipitation, snowmelt, or other sources
426 that flows over the land surface, and is a major component of the hydrological cycle. Overall
427 changes in surface runoff are similar to those in precipitation, accompanied by contributions from
428 changes in snowmelt. For the mountain tops, warming of 0.22 K is found attributed to ASI (0.12
429 K) and ACI (0.17 K) associated with local dust and anthropogenic aerosols, respectively, with 10%
430 or more reduction in precipitation, snowpack, and surface runoff. Therefore, aerosols may
431 contribute to California drought through both the warming of mountain tops and anomalously low
432 precipitation over the whole area. For the lower elevations, the domain averaged changes are
433 similar to those for the whole domain, except for SWE which slightly increases by 0.42% due to
434 ARI (2.43%) with main contribution from transported aerosols (4.01%).

435 The simulations for year 2013-2014 are consistent with those in year 2012-2013 (Table 4).
436 For the whole domain in year 2013-2014, temperature is cooled by 0.21 K due to aerosols,

accompanied by reduction in precipitation, SWE, and surface runoff of about 6%, 9%, and 5%, respectively. Aerosol impacts on SWE is more significant in year 2013-2014 (–8.88%) than in year 2012-2013 (–3.17%), possibly due to less precipitation and SWE in year 2013-2014 than year 2012-2013 (not shown). The changes of SWE for year 2013-2014 are −15.57% for the mountain tops and 2.66% for the lower elevations. The relative change of surface runoff at the mountain tops in year 2013-2014 is smaller than year 2012-2013 because the mean surface runoff in year 2013-2014 (0.33 mm $day^{-1}$) is larger than that in year 2012-2013 (0.27 mm $day^{-1}$), possibly contributed by less SWE and faster snowmelt at the mountain tops in year 2013-2014. The corresponding changes in evapotranspiration are –0.12% in year 2012-2013 and –1.20% in year 2013-2014, respectively, which also contributes to the relatively smaller change of surface runoff in year 2013-2014 at the mountain tops.

### 3.3 Seasonal Variations of Aerosol Effects

Figure 13 depicts the monthly mean AOD for total aerosols (brown solid), local anthropocentric aerosols (green dashed), local dust (blue dashed), and transported aerosols (red dashed) averaged over the whole domain, mountain tops, and lower elevation area from October 2012 to June 2013. It is seen that transported aerosols contribute to about two-thirds of the total AOD. The total AOD has two maxima, one in December and one in May, mainly associated with the seasonal variations of transported aerosols and local dust aerosols. Local dust AOD starts to increase in March and reaches a maximum around May, while transported aerosol AOD peaks in April (Fig. 13a). The seasonal variations of AOD over the mountain tops and lower elevations are similar to those of the whole domain (Figs. 13b and 13c).

459 The monthly mean differences in precipitation due to the total aerosols (brown solid), ARI
460 (green solid), ASI (blue solid), ACI (red solid), local anthropocentric aerosols (green dashed), local
461 dust (blue dashed), and transported aerosols (red dashed) are shown in Fig. 14. Reduced
462 precipitation is seen over the whole domain, with the most contribution from transported aerosols,
463 followed by local anthropogenic aerosols, both of which play roles in precipitation changes
464 through ACI as previously shown. ARI, ASI, or locally emitted dust aerosols do not seem to play
465 an important role in the monthly mean precipitation changes (Fig. 14a). Two maxima of aerosol
466 effects are found: one in December when it is the rainy season of the California (Fig. 3a) and at
467 the same time relatively larger AOD presents over this region (Fig. 13a); the other peak reduction
468 in precipitation due to the aerosol effects is found in May with a value of about 0.2 mm $day^{-1}$ (Fig.
469 13a), probably associated with the maximum aerosols (Fig. 13a) and also the orographic
470 precipitation over the mountain region during that time period (Lee et al., 2015). Given that the
471 monthly mean precipitation in May is only about 1 mm $day^{-1}$ (Fig. 3a), the reduction caused by
472 aerosols is about 20%. For monthly mean precipitation, changes over the mountain tops and the
473 lower elevation area, respectively, have similar seasonal variation patterns (Figs. 14b and 14c).
474 For SWE, however, changes over the mountain tops are different from those in the lower
475 area (Fig. 15). For mountain tops, negative changes in SWE are seen over the whole time period,
476 with a maximum reduction of about 60 mm in May corresponding to the maximum AOD (Fig.
477 15b). Major contribution is from local dust aerosols through ASI, as well as transported and local
478 anthropogenic aerosols through ACI. ARI produces small positive changes (~ 5 mm in May) in
479 SWE due to the scattering and absorption of solar radiation by aerosols which leads to surface
480 cooling. For lower elevation area, slightly enhanced SWE is found during the winter time,
481 associated with the effects of transported aerosols which produce more clouds through ACI, and

together with the ARI effect, lead to the cooling of the surface and hence less snowmelt (Fig. 15c). Over the whole domain, SWE is reduced with a maximum of about 2 mm in May, equivalent to about 2% reduction, mainly attributed to the local dust particles through ASI, and local anthropogenic and transported aerosols through ACI (Fig. 15a).

Changes in temperature also exhibit different patterns over the mountain tops and the lower elevations (Fig. 16). Warming over the mountain tops is produced by dust aerosols through ASI with a maximum around May, and by transported aerosols through ACI during winter which leads to reduced precipitation and SWE with a maximum in January (Fig. 16b). Cooling over the lower elevation areas is caused by ARI, and also induced by more clouds generated in the model simulations due to transported aerosols through ACI, with a maximum cooling of about 0.3 K in April, corresponding to the maximum AOD of transported aerosols (Fig. 16c). The average temperature changes over the whole domain are negative because of the large area of the lower elevations (Fig. 16a).

Surface runoff reaches a maximum in December for the lower elevations and the whole domain, but a peak value in May for mountain tops when the temperature is warmer (Fig. S4). For lower elevations where there is not much snow, surface runoff is mainly associated with precipitation and the changes present a similar pattern to those in precipitation (Fig. 17c). Changes in surface runoff for the whole area present similar patterns to those of the lower elevations because of the larger area of lower elevations (Fig. 17a). However for mountain tops, changes in surface runoff are also associated with changes in snowmelt. Surface runoff over the mountain tops shows a slight increase in spring, and then a decrease after April (Fig. 17b). The increase can be explained by the effect of local dust aerosols deposited on the snow, which reduces the snow albedo through ASI and warms the surface, leading to more and earlier snowmelt than normal, consistent with

505 negative changes in SWE. The decrease after April is a combined effect of less snowpack available
506 for melting caused by earlier snowmelt due to local dust aerosols and reduced precipitation caused
507 by transported and local anthropogenic aerosols through ACI. Thus, the impact of aerosols is to
508 speed up snowmelt at the mountain tops in spring and modify the seasonal cycle of surface runoff.
509

510 ## 4. Conclusions

511 A fully coupled high-resolution aerosol-meteorology-snowpack model is employed to
512 investigate the impacts of various aerosol sources on precipitation and snowpack in California.
513 The relative roles of locally emitted anthropogenic and dust aerosols, and aerosols transported
514 from outside the model domain are differentiated through the three pathways, aerosol-radiation
515 interaction (ARI), aerosol-snow interaction (ASI), and aerosol-cloud interaction (ACI). In the
516 following summary, the numbers in brackets represent the domain averaged changes (Table 4).

517 **Temperature**: Local dust aerosols warm the mountain top surface through ASI (0.12 K), in
518 which the reduced snow albedo associated with dirty snow leads to more surface absorption of
519 solar radiation. Transported and local anthropogenic aerosols warm the surface of mountain tops
520 through ACI (0.17 K), which produces more non-precipitating clouds but reduces precipitation
521 and hence snow amount, leading to decreased surface albedo and more absorption of solar energy.
522 The cooling of the valley area (–0.21 K) is primarily caused by the scattering and absorption of all
523 aerosols through ARI (–0.14 K). Transported and anthropogenic aerosols can also cool the surface
524 over the central valley through ACI (–0.07 K) that enhances cloud amount, leading to more
525 reflection of solar radiation.

526 **Precipitation and SWE**: Reduced precipitation of –6.87% is found due to the aerosol effects
527 and is mainly caused by transported and local anthropogenic aerosols through ACI (–6.26%). The

maximum of aerosol effect on precipitation is found in December during the rainy season when the aerosols loadings are also relatively large. The other peak effect occurs in May with a reduction of about 20%, probably associated with the maximum of aerosol loadings and more orographic precipitation over the mountains. Locally emitted dust aerosols represent one of the most important contributors to the reduced SWE (–3.17%) through ASI (–1.96%), with the largest reduction in May corresponding to the maximum dust emission over that time. Local anthropogenic aerosols can also reduce SWE through ACI (–2.67%). On the other hand, ARI (2.43%) by all aerosols, with most contributions from the transported aerosols, exceeds the effects of ASI (–0.99%) and ACI (–0.27%) and slightly enhance SWE by 0.42% over lower elevations in winter time through the surface cooling.

**Surface runoff**: As a major component of the water cycle, surface runoff is mainly generated by precipitation, but for mountain tops, the changes in surface runoff are also associated with the changes in snowmelt. We find that the seasonal-mean surface runoff is reduced by –6.58% associated with suppressed precipitation, caused by transported and anthropogenic aerosols through ACI (–6.30%). Over mountain tops, runoff slightly increases in spring due to the enhanced solar absorption by dust aerosols. Runoff decreases after April as a combined effect of less snowpack available for melting caused by earlier snowmelt due to local dust and reduced precipitation due to transported and local anthropogenic aerosols through ACI. Therefore, one of the important impacts of aerosols is to speed up the snowmelt at mountain tops in spring and modify the seasonal cycle of surface runoff.

In summary, we find that the WRF-Chem model simulations with aerosol effects included would produce lower precipitation and SWE by about 10% and colder temperature by 0.2 K over California than the simulations without aerosols. Therefore, including aerosol effects can reduce

551 the high biases of these variables in the simulations reported previously. Aerosols play an
552 important role in California water resources through the warming of mountain tops and the
553 subsequent modification of precipitation and snowmelt. The total aerosol effects produce a
554 warming of 0.22 K over mountain tops and a reduction from October to June in precipitation, SWE,
555 and surface runoff of about 7%, 3%, and 7%, respectively, for the whole domain, with
556 corresponding numbers of 10% or more over mountain tops. In a dry year (year 2013-2014),
557 aerosol can have more significant impacts on SWE, with a reduction of up to 9% for the whole
558 domain and 16% over mountain tops.

559 It is challenging to accurately represent aerosol properties in the model (Fast et al., 2014).
560 As pointed out by Wu et al. (2017), biases exist in the current model as compared to observations,
561 for example, underestimation of AOD due to poor representation of dust emission and vertical
562 mixing in the warm season. The underestimate of AOD in the model implies that the simulated
563 aerosol effects could also be biased low. Given the important role that dust plays in the California
564 snowpack, improved dust emission and vertical mixing are needed for accurate quantification of
565 the impact of dust. Also, the underestimation of organic matter (associated with secondary organic
566 aerosol processes) in the model (Wu et al., 2017), which are primarily scattering aerosols, would
567 contribute to the high bias in the simulation of surface temperature. More accurate representation
568 and simulation of these aerosols in the model are needed. In the current WRF-Chem model, the
569 aerosol effect on ice clouds is not included. ACI associated with ice clouds are more complex than
570 that with liquid clouds. For example, a few studies have shown that negative Twomey effects may
571 occur with aerosols and ice clouds, in which increased aerosols (and thus ice nuclei) lead to
572 enhanced heterogeneous nucleation that is associated with larger and fewer ice crystals as
573 compared to the homogeneous nucleation counterpart (DeMott et al., 2010; Chylek et al., 2006,

Zhao et al. 2018). A recent study shows that the responses of ice crystal effective radius to aerosol loadings are modulated by water vapor amount in conjunction with several other meteorological parameters. While there is a significant negative correlation between ice effective radius and aerosol loading in moist conditions, consistent with the "Twomey effect" for liquid clouds, a strong positive correlation between the two occurs in dry conditions (Zhao et al. 2018). Despite numerous studies about the impact of aerosols on ice clouds, the role of anthropogenic aerosols in ice processes, especially over polluted regions, remains a challenging scientific issue. The effect of anthropogenic aerosols on ice formation and cloud radiative properties may be a critical pathway through which anthropogenic activities affect regional climate and present the opportunities for further studies using observations and models.

Our model simulation produces relative larger SWE than the SNOTEL observations. Improvement of snowpack simulation in the land surface model is needed for accurate quantification of aerosol impacts on snowpack. Our results are based on two years of simulations. Additional simulations under different meteorological conditions will help to better assess the aerosol impacts on California hydrology quantitatively.

## Data availability

The PRISM data are available through the following link: http://prism.oregonstate.edu/recent/. The CPC data are available through the following link: https://www.esrl.noaa.gov/psd/data/gridded/data.unified.daily.conus.html. The DWR data are available through the following link: http://cdec.water.ca.gov/snow_rain.html. The CIMIS data are available through the following link: http://wwwcimis.water.ca.gov/. The SNOTEL data are available through the following link: https://www.wcc.nrcs.usda.gov/snow/. The MISR data is

597 available through the following link: https://misr.jpl.nasa.gov/getData/accessData/. The NLDAS
598 MOS0125 albedo data are available through the following link:
599 https://giovanni.gsfc.nasa.gov/giovanni/#service=TmAvMp&starttime=&endtime=&variableFac
600 ets=dataFieldMeasurement%3AAlbedo%3BdataProductPlatformInstrument%3ANLDAS%20M
601 odel%3BdataProductTimeInterval%3Amonthly%3B.
602

603 ## Competing interests

604 The authors declare that they have no conflict of interest.
605

606 ## Acknowledgements

607 This study was carried out at the Joint Institute for Regional Earth System Science and Engineering
608 and Department of Atmospheric and Oceanic Science, University of California, Los Angeles, and
609 sponsored by California Energy Commission under grant #EPC-14-064. LW, JHJ, HS, and YSC
610 conducted the work at the Jet Propulsion Laboratory, California Institute of Technology, under
611 contract with the National Aeronautics and Space Administration. They acknowledge the funding
612 support from the NASA ACMAP program. CZ is supported by the "Thousand Talents Plan for
613 Young Professionals" program of China. The contribution of YQ is supported by the U.S.
614 Department of Energy (DOE), Office of Science, Biological and Environmental Research as part
615 of the Regional and Global Climate Modeling Program. The Pacific Northwest National
616 Laboratory (PNNL) is operated for DOE by Battelle Memorial Institute under contract DE-AC05-
617 76RL01830. We would like to thank two anonymous reviewers for their constructive comments
618 and suggestions for the improvement of this paper.
619

620 ## References


621 Ault, A. P., Williams, C. R., White, A. B., Neiman, P. J., Creamean, J. M., Gaston, C. J., Ralph,
622 F. M., and Prather K. A.: Detection of Asian dust in California orographic precipitation, J.
623 Geophys. Res., 116, D16205, doi:10.1029/2010JD015351, 2011.

624 Binkowski, F. S. and Shankar, U.: The Regional Particulate Matter Model: 1. Model description
625 and preliminary results, J. Geophys. Res., 100: doi: 10.1029/95JD02093. issn: 0148-0227,
626 1995.

627 Bishop, J. K. B., Davis, R. E., and Sherman J. T.: Robotic observations of dust storm enhancement
628 of carbon biomass in the North Pacific, Science, 298, 817–821, doi:10.1126/science.1074961,
629 2002.

630 Barnard, J. C., Fast, J. D., Paredes-Miranda, G., Arnott, W. P., and Laskin, A.: Technical Note:
631 Evaluation of the WRF-Chem "Aerosol Chemical to Aerosol Optical Properties" Module
632 using data from the MILAGRO campaign, Atmos. Chem. Phys., 10, 7325–7340,
633 doi:10.5194/acp-10-7325-2010, 2010.

634 Brandt, R. E., Warren, S. G., and Clarke, A. D.: A controlled snowmaking experiment testing the
635 relation between black-carbon content and reduction of snow albedo, J. Geophys. Res. 116,
636 D08109, 2011.

637 Chadwick, O. A., Derry, L. A., Vitousek, P. M., Huebert, B. J., and Hedin L. O.: Changing sources
638 of nutrients during four million years of ecosystem development, Nature, 397, 491–497,
639 doi:10.1038/17276, 1999.

640 Charlson, R. J., Schwartz, S. E., Hales, J. H., Cess, R. D., Coakley Jr., J. A., Hansen, J. E., and
641 Hofmann D. J.: Climate forcing by anthropogenic aerosols, Science, 255, 423–430,
642 doi:10.1126/science.255.5043.423, 1992.

643 Chapman, E. G., Gustafson Jr., W. I., Easter, R. C., Barnard, J. C., Ghan, S. J., Pekour, M. S., and
644 Fast, J. D.: Coupling aerosolcloud-radiative processes in the WRF-Chem model:
645 Investigating the radiative impact of elevated point sources, Atmos. Chem. Phys., 9, 945–
646 964, doi:10.5194/acp-9-945-2009, 2009.
647 Chen, M., Xie, P., and Co-authors: CPC Unified Gauge-based Analysis of Global Daily
648 Precipitation, Western Pacific Geophysics Meeting, Cairns, Australia, 29 July - 1 August,
649 2008.
650 Creamean, J. M., Suski, K. J., Rosenfeld, D., Cazorla, A., DeMott, P. J., Sullivan, R. C., White, A.
651 B., Ralph, F. M., and Prather, K. A.: Dust and biological aerosols from the Sahara and Asia
652 influence precipitation in the western US, Science, 339(6127), 1572–1578,
653 doi:10.1126/science.1227279, 2013.
654 Creamean, J. M., Ault, A. P., White, A. B., Neiman, P. J., Ralph, F. M., Minnis, P., and Prather,
655 K. A.: Impact of interannual variations in sources of insoluble aerosol species on orographic
656 precipitation over California's central Sierra Nevada, Atmos. Chem. Phys., 15, 6535-6548,
657 doi:10.5194/acp-15-6535-2015, 2015.
658 Diner, D. J., Beckert, J. C., Reilly, T. H., Bruegge, C. J., Conel, J. E., Kahn, R. A., Martonchik, J.
659 V., Ackerman, T. P., Davies, R., Gerstl, S. A.W., Gordon, H. R., Muller, J. P., Myneni, R.
660 B., Sellers, P. J., Pinty, B., and Verstraete, M. M.: Multi-angle Imaging SpectroRadiometer
661 (MISR) Instrument Description and Experiment Overview, IEEE T. Geosci. Remote, 36,
662 1072–1087, 1998.
663 Durkee, P. A., Chartier, R. E., Brown, A., Trehubenko, E. J., Rogerson, S. D., Skupniewicz, C.,
664 Nielsen, K. E., Plantnick, S, and King, M. D.: Composite ship track characteristics, J. Atmos.
665 Sci., 57, 2542-2553, 2000.

666 Easter, R. C., et al.: MIRAGE: Model description and evaluation of aerosols and trace gasses. J.
667 Geophys. Res., 109, D20210, doi:10.1029/ 2004JD004571, 2004.
668 Emmons, L. K., Walters, S., Hess, P. G., Lamarque, J.-F., Pfister, G. G., Fillmore, D., Granier, C.,
669 Guenther, A., Kinnison, D., Laepple, T., Orlando, J., Tie, X., Tyndall, G., Wiedinmyer, C.,
670 Baughcum, S. L., and Kloster, S.: Description and evaluation of the Model for Ozone and
671 Related chemical Tracers, version 4 (MOZART-4), Geosci. Model Dev., 3, 43–67,
672 https://doi.org/10.5194/gmd-3-43-2010, 2010.
673 Fan, J., Leung, L. R., DeMott, P. J., Comstock, J. M., Singh, B., Rosenfeld, D., Tomlinson, J. M.,
674 White, A., Prather, K. A., Minnis, P., Ayers, J. K., and Min, Q.: Aerosol impacts on
675 California winter clouds and precipitation during CalWater 2011: local pollution versus long-
676 range transported dust, Atmos. Chem. Phys., 14, 81-101, doi:10.5194/acp-14-81-2014, 2014.
677 Fast, J. D., Gustafson Jr., W. I., Easter, R. C., Zaveri, R. A., Barnard, J. C., Chapman, E. G., Grell,
678 G. A. and Peckham, S. E.: Evolution of ozone, particulates, and aerosol direct radiative
679 forcing in the vicinity of Houston using a fully coupled meteorology-chemistry-aerosol
680 model, J. Geophys. Res., 111, D21305, doi:10.1029/2005JD006721, 2006.
681 Fast, J. D., Allan, J., Bahreini, R., Craven, J., Emmons, L., Ferrare, R., Hayes, P. L., Hodzic, A.,
682 Holloway, J., Hostetler, C., Jimenez, J. L., Jonsson, H., Liu, S., Liu, Y., Metcalf, A.,
683 Middlebrook, A., Nowak, J., Pekour, M., Perring, A., Russell, L., Sedlacek, A., Seinfeld, J.,
684 Setyan, A., Shilling, J., Shrivastava, M., Springston, S., Song, C., Subramanian, R., Taylor,
685 J. W., Vinoj, V., Yang, Q., Zaveri, R. A., and Zhang, Q.: Modeling regional aerosol and
686 aerosol precursor variability over California and its sensitivity to emissions and long-range
687 transport during the 2010 CalNex and CARES campaigns, Atmos. Chem. Phys., 14, 10013-
688 10060, doi:10.5194/acp-14-10013-2014, 2014.

689 Flanner, M. G., and Zender, C. S.: Snowpack radiative heating: Influence on Tibetan Plateau
690 climate, Geophys. Res. Lett., 32, L06501, doi:10.1029/2004GL022076, 2005.
691 Flanner, M. G., Zender, C. S., Randerson, J. T., and Rasch, P. J.: Present-day climate forcing and
692 response from black carbon in snow, J. Geophys. Res., 112, D11202,
693 doi:10.1029/2006JD008003, 2007.
694 Flanner, M. G., Zender, C. S., Hess, P. G., Mahowald, N. M., Painter, T. H., Ramanathan, V., and
695 Rasch, P. J.: Springtime warming and reduced snow cover from carbonaceous particles,
696 Atmos. Chem. Phys., 9, 2481-2497, doi:10.5194/acp-9-2481-2009, 2009.
697 Flanner, M. G., Liu, X., Zhou, C., Penner, J. E., and Jiao, C. (2012), Enhanced solar energy
698 absorption by internally-mixed black carbon in snow grains, Atmos. Chem. Phys., 12, 4699-
699 4721, doi:10.5194/acp-12-4699-2012, 2012.
700 Graham, W. F., and Duce, R. A.: The atmospheric transport of phosphorus to the western North ‐
701 Atlantic, Atmos. Environ., 16, 1089 ‐ 1097, doi:10.1016/0004-6981(82)90198-6, 1982.
702 Grell, G., Peckham, S., Schmitz, R., et al.: Fully coupled “online” chemistry within the WRF
703 model, Atmos. Environ., 39(37), 6957–6975, 2005.
704 Griffin, D., and Anchukaitis, K. J.: How unusual is the 2012–2014 California drought?, Geophys.
705 Res. Lett., 41, 9017–9023, doi:10.1002/2014GL062433, 2014.
706 Gu, Y., Liou, K. N., Xue, Y., Mechoso, C. R., Li, W., and Luo, Y.: Climatic effects of different
707 aerosol types in China simulated by the UCLA general circulation model, J. Geophys. Res.,
708 111, D15201, doi:10.1029/2005JD006312, 2006.
709 Gu, Y., Liou, K. N., Lee, W.-L., and Leung, L. R.: Simulating 3-D radiative transfer effects over
710 the Sierra Nevada Mountains using WRF, Atmos. Chem. Phys., 12, 9965–9976,
711 doi:10.5194/acp-129965-2012, 2012a.

712 Gu, Y., Liou, K. N., Jiang, J. H., Su, H., and Liu, X.: Dust aerosol impact on North Africa climate:
713 a GCM investigation of aerosol-cloud-radiation interactions using A-Train satellite data,
714 Atmos. Chem. Phys., 12, 1667-1679, doi:10.5194/acp-12-1667-2012, 2012b.Gu, Y., Xue, Y.,
715 De Sales, F., and Liou, K. N.: A GCM investigation of dust aerosol impact on the regional
716 climate of North Africa and South/East Asia, Clim. Dyn, 46, 2353-2370, doi
717 10.1007/s00382-015-2706-y, 2016.
718 Gu, Y., Liou, K. N., Jiang, J. H., Fu, R., Lu, S., and Xue, Y.: A GCM investigation of impact of
719 aerosols on the precipitation in Amazon during the dry to wet transition, Clim. Dyn,,
720 48:2393-2404, doi:10.1007/s00382-016-3211-7, 2017.
721 Gustafson, W. I., Chapman, E. G., Ghan, S. J., Easter, R. C., and Fast, J. D.: Impact on modeled
722 cloud characteristics due to simplified treatment of uniform cloud condensation nuclei during
723 NEAQS 2004, Geophys. Res. Lett., 34, L19809, doi:10.1029/2007GL030021, 2007.
724 Hansen, J., Sato, M., and Ruedy, R.: Radiative forcing and climate response, J. Geophys. Res.,
725 102, 6831– 6864, doi:10.1029/96JD03436, 1997.
726 Hadley, O. L., Corrigan, C. E., Kirchstetter, T. W., Cliff, S. S., and Ramanathan, V.: Measured
727 black carbon deposition on the Sierra Nevada snow pack and implication for snow pack
728 retreat, Atmos. Chem. Phys., 10, 7505-7513, doi:10.5194/acp-10-7505-2010, 2010.
729 Hadley, O. L., and Kirchstetter, T. W.: Black-carbon reduction of snow albedo. Nature Climate
730 Change, 2, 437-440, doi:10.1038/nclimate1433, 2012.
731 Hess, M., Koepke, P., and Schult, I.: Optical Properties of Aerosols and Clouds: The Software
732 Package OPAC, Bull. Amer. Meteor. Soc., 79, 831–844,
733 doi:10.1175/15200477(1998)079<0831:OPOAAC>2.0.CO;2, 1998.

734 Hu, Z., C. Zhao, J. Huang, L. R. Leung, Y. Qian, H. Yu, L. Huang, O. V. Kalashnikova (2016):
735 Trans-pacific transport and evolution of aerosols: Evaluation of quasi-global WRF-Chem
736 simulation with multiple observations, Geosci. Model Dev., 9, 1725–1746, 2016.
737 Jacobson, M. Z.: Climate response of fossil fuel and biofuel soot, accounting for soot's feedback
738 to snow and sea ice albedo and emissivity, J. Geophys. Res., 109( D21201),
739 doi:10.1029/2004JD004945, 2004.
740 Jiang, H., and Feingold, G.: Effect of aerosol on warm convective clouds: Aerosol-cloud-surface
741 flux feedbacks in a new coupled large eddy model, J. Geophys. Res., 111, D01202,
742 doi:10.1029/2005JD006138, 2006.
743 Jiang, J.H., Livesey, N.J., Su, H., Neary, L., McConnell, J.C., and Richards, N.A.: Connecting
744 surface emissions, convective uplifting, and long-range transport of carbon monoxide in the
745 upper-troposphere: New observations from the Aura Microwave Limb Sounder, *Geophys.*
746 *Res. Lett.* 34, L18812, doi:10.1029/2007GL030638, 2007.
747 Johnson,J.B.,and Marks, D.:Thedetectionandcorrectionof snow-water equivalent pressure sensor
748 errors, Hydrol. Processes, 18, 3513–3525, 2004.
749 Kiehl, J. and Briegleb, B.: The relative roles of sulfate aerosols and greenhouse gases in climate
750 forcing, Science, 260, 311-314, 1993.
751 Kim, J., Gu, Y., and Liou, K.-N.: The impact of the direct aerosol radiative forcing on surface
752 insolation and spring snowmelt in the southern Sierra Nevada, J. Hydrometeorol., 7, 976-
753 983, 2006.
754 Koren, I., Kaufman, Y. J., Remer, L. A., and Martins, J. V.: Measurement of the effect of Amazon
755 smoke on inhibition of cloud formation, Science, 303, 1342–1345,
756 doi:10.1126/science.1089424, 2004.

Lee, W.-L. and Liou, K. N.: Effect of absorbing aerosols on snow albedo reduction in the Sierra Nevada. Atmospheric Environment, 55, 425–430. doi:10.1016/j.atmosenv.2012.03.024, 2012.

Lee, W.-L., Gu, Y., Liou, K. N., Leung, L. R., and Hsu, H.-H.: A global model simulation for 3-D radiative transfer impact on surface hydrology over the Sierra Nevada and Rocky Mountains, Atmos. Chem. Phys., 15, 5405–5413, doi:10.5194/acp-15-54052015, 2015.

Leung, L. R., Qian, Y., Bian, X., Washington, W. M., Han, J., and Roads, J. O.: Mid-century ensemble regional climate change scenarios for the western United States, Climatic Change, 62, 75– 113, 2004.

Liou, K. N., Gu, Y., Leung, L. R., Lee, W. L., and Fovell, R. G.: A WRF simulation of the impact of 3-D radiative transfer on surface hydrology over the Rocky Mountains and Sierra Nevada, Atmos. Chem. Phys., 13, 11709–11721, doi:10.5194/acp-1311709-2013, 2013.

Lynn, B., Khain, A., Rosenfeld, D., and Woodley, W. L.: Effects of aerosols on precipitation from orographic clouds, J. Geophys. Res., 112, D10225, doi:10.1029/2006JD007537, 2007.

Mills, M. M., Ridame, C., Davey, M., La Roche, J., and Geider, R. J.: Iron and phosphorus co‐limit nitrogen fixation in the eastern tropical North Atlantic, Nature, 429, 292‐294, doi:10.1038/nature02550, 2004.

Oaida, C. M., Xue, Y., Flanner, M. G., Skiles, S. M., De Sales, F., and Painter, T. H.: Improving snow albedo processes in WRF/SSiB regional climate model to assess impact of dust and black carbon in snow on surface energy balance and hydrology over western U.S., J. Geophys. Res. Atmos., 120, 3228–3248. doi: 10.1002/2014JD022444, 2015.

778 Painter, T. H., Barrett, A. P., Landry, C. C., Neff, J. C., Cassidy, M. P., Lawrence, C. R., McBride,
779 K. E., and Farmer, G. L.: Impact of disturbed desert soils on duration of mountain snow
780 cover, Geophys. Res. Lett., 34, L12502, doi:10.1029/2007GL030284, 2007.
781 Painter, T. H., Deems, J. S., Belnap, J., Hamlet, A. F., Landry, C. C., Udall, B.: Response of
782 Colorado River runoff to dust radiative forcing in snow, Proceedings of the National
783 Academy of Sciences, 2010, 107, 40, 17125, 2010.
784 Pepin, N., Bradley, R. S., Diaz, H. F., Baraer, M., Caceres, E. B., Forsythe, N., H. Fowler, H.,
785 Greenwood, G., Hashmi, M. Z., Liu, X. D., Miller, J. R., Ning, L., Ohmura, A., Palazzi, E.,
786 Rangwala, I., Schöner, W., Severskiy, I., Shahgedanova, M., Wang, M. B., Williamson, S.
787 N., Yang. D. Q.: Elevation-dependent warming in mountain regions of the world, Nature
788 Climate Change, 5 (5), 424, DOI: 10.1038/nclimate2563, 2015.
789 Platnick, S., and Twomey, S.: Determining the susceptibility of cloud albedo to changes in droplet
790 concentration with the Advanced Very High Resolution Radiometer, J. Appl. Meteor., 33,
791 334-347, 1994.
792 PRISM Climate Group, Oregon State University, http://prism.oregonstate.edu, created 4 Feb 2004.
793 Qian Y, Leung, L. R., Ghan, S. J., and Giorgi, F.: Regional Climate Effects of Aerosols Over China:
794 Modeling and Observation, Tellus Series B, Chemical and Physical Meteorology 55(4):914-
795 934, 2003.
796 Qian, Y., Gustafson Jr., W. I., Leung, L. R., and Ghan, S. J.: Effects of soot-induced snow albedo
797 change on snowpack and hydrological cycle in western United States based on Weather
798 Research and Forecasting chemistry and regional climate simulations, J. Geophys. Res., 114,
799 D03108, doi:10.1029/2008JD011039, 2009a.

Qian, Y., Gong, D., Fan, J., Leung, L. R., Bennartz, R., Chen, D, and Wang, W.: Heavy pollution suppresses light rain in China: observations and modeling, J. Geophys. Res. D. (Atmospheres) 114:article number D00K02, doi:10.1029/2008JD011575, 2009b.

Qian, Y., Flanner, M. G., Leung, L. Y. R., and Wang, W.: Sensitivity studies on the impacts of Tibetan Plateau snowpack pollution on the Asian hydrological cycle and monsoon climate, Atmos. Chem. Phys., 11(5):1929-1948. doi:10.5194/acp-11-1929-2011, 2011.

Qian, Y., Yasunari, T. J., Doherty, S. J., Flanner, M. G., Lau, W. K., Ming, J., Wang, H., Wang, M., Warren, S. G., and Zhang, R.: Light-absorbing Particles in Snow and Ice: Measurement and Modeling of Climatic and Hydrological Impact, Advances in Atmospheric Sciences 32(1):64-91, doi:10.1007/s00376-014-0010-0, 2015.

Rasmussen, R. M. and Coauthors: Weather Support to Deicing Decision Making (WSDDM): A winter weather nowcasting system, Bull. Amer. Meteor. Soc., 82, 579–595, 2001.

Rosenfeld, D., Woodley, W. L., Axisa, D., Freud, E., Hudson, J. G., and Givati, A.: Aircraft measurements of the impacts of pollution aerosols on clouds and precipitation over the Sierra Nevada, J. Geophys. Res., 113, D15203, doi:10.1029/2007JD009544, 2008a.

Rosenfeld, D., Lohmann, U., Raga, G. B., O'Dowd, C. D., Kulmala, M., Fuzzi, S., Reissell, A., and Andreae, M. O.: Flood or drought: How do aerosols affect precipitation?, Science, 321, 1309–1313, doi:10.1126/science.1160606, 2008b.

Serreze, M. C., Clark, M. P., Armstrong, R. L., McGinnis, D. A., and Pulwarty, R. S.: Characteristics of the western United States snowpack from snowpack telemetry (SNOTEL) data. Water Resour. Res., 35, 2145–2160, 1999.

821 Serreze, M. C., Clark, M. P., and Frei, A.: Characteristics of large snowfall events in the montane
822 western United States as examined using snowpack telemetry (SNOTEL) data. Water Resour.
823 Res., 37, 675–688, 2001.
824 Sheffield, J., Pan, M., Wood, E.F., Mitchell, K.E., Houser, P.R., Schaake, J.C., Robock, A.,
825 Lohmann, D., Cosgrove, B., Duan, Q., Luo, L., Higgins, R.W., Pinker, R.T., Dan Tarpley,
826 J., and Ramsay, B.H.: Snow process modeling in the North American Land Data
827 Assimilation System (NLDAS): 1. Evaluation of model-simulated snow cover extent, J.
828 Geophys. Res., 108(D22), 8849, doi:10.1029/2002JD003274, 2003.
829 Shindell, D.T., Pechony, O., Voulgarakis, A., Faluvegi, G., Nazarenko, L., Lamarque, J.-F.,
830 Bowman, K., Milly, G., Kovari, B., Ruedy, R., and Schmidt, G.: Interactive ozone and
831 methane chemistry in GISS-E2 historical and future climate simulations. Atmos. Chem.
832 Phys., 13, 2653-2689, doi:10.5194/acp-13-2653-2013, 2013.
833 Snyder, R. L.: California irrigation management information system. Am. J. Potato Res. 61(4):
834 229 – 234, 1984.
835 Sokolik, I. N., Winker, D. M., Bergametti, G., Gillette, D. A., Carmichael, G., Kaufman, Y. J.,
836 Gomes, L., Schuetz, L., and Penner, J. E.: Introduction to special section: Outstanding
837 problems in quantifying the radiative impacts of mineral dust, J. Geophys. Res., 106(D16),
838 18,015 – 18,027, doi:10.1029/2000JD900498, 2001.
839 Toon, O.B., McKay, C.P., Ackerman, T.P. and Santhanam, K.: Rapid calculation of radiative
840 heating rates and photodissociation rates in inhomogeneous multiple scattering atmospheres.
841 Journal of Geophysical Research 94: doi: 10.1029/89JD01321. issn: 0148-0227, 1989.
842 Twomey, S.: The influence of pollution on the shortwave albedo of clouds. J. Atmos. Sci., 34,
843 1149-1152, 1977.

844 VanCuren, R. A.: Asian aerosols in North America: Extracting the chemical composition and mass
845 concentration of the Asian continental aerosol plume from long-term aerosol records in the
846 western United States, J. Geophys. Res., 108, 4623, doi:10.1029/2003JD003459, D20, 2003.
847 VanCuren, R.A., Cliff, S.S., Perry, K.D. and Jimenez-Cruz, M.: Asian continental aerosol
848 persistence above the marine boundary layer over the eastern North Pacific: Continuous
849 aerosol measurements from Intercontinental Transport and Chemical Transformation 2002
850 (ITCT 2K2), J. Geophys. Res., 110: doi: 10.1029/2004JD004973, issn: 0148-0227, 2005.
851 Vicars, W. C., and Sickman, J. O.: Mineral dust transport to the Sierra Nevada, California: Loading
852 rates and potential source areas, J. Geophys. Res., 116, G01018, doi:10.1029/2010JG001394,
853 2011.
854 Waliser, D. E., and Coauthors: Simulating the Sierra Nevada snowpack: The impact of snow
855 albedo and multi-layer snow physics, Climatic Change, 109 (Suppl. 1), S95–S117,
856 doi:10.1007/s10584-011-0312-5, 2011.
857 Wang, Y., Jiang, J. H. and Su, H.: Atmospheric Responses to the Redistribution of Anthropogenic
858 Aerosols, J. Geophys. Res. Atmos., 120, 9625-9641, doi:10.1002/2015JD023665, 2015.
859 Wang, Y., Wang, M., Zhang, R., Ghan, S.J., Lin, Y., Hu, J., Pan, B., Levy, M., Jiang, J.H., and
860 Molina, M.J.: Assessing the effects of anthropogenic aerosols on Pacific storm track using a
861 multiscale global climate model, Proc. Nat. Acad. Sci. 111, 19, 6894–6899, doi:
862 10.1073/pnas.1403364111, 2014.
863 Warren, S., and Wiscombe W.: Dirty snow after nuclear war, Nature, 313, 467–470, 1985.
864 Wiscombe, W. J. and Warren, S. G.: A model for the spectral albedo of snow, I: Pure snow, J.
865 Atmos. Sci., 37, 2712–2733, 1980.

866 Wu, L., Su, H., and Jiang, J. H.: Regional simulations of deep convection and biomass burning
867 over South America: 2. Biomass burning aerosol effects on clouds and precipitation, J.
868 Geophys, Res. Atmos., 116, doi:10.1029/2011JD016106, 2011.
869 Wu, L., Su, H., and Jiang, J. H.: Regional simulation of aerosol impacts on precipitation during
870 the East Asian summer monsoon, J. Geophys. Res. Atmos., 118, 6454–6467,
871 doi:10.1002/jgrd.50527, 2013.
872 Wu, L., Su, H., Kalashnikova, O. V., Jiang, J. H., Zhao, C., Garay, M. J., Campbell, J. R., and Yu,
873 N.: WRF-Chem simulation of aerosol seasonal variability in the San Joaquin Valley, Atmos.
874 Chem. Phys., 17, 7291-7309, https://doi.org/10.5194/acp-17-7291-2017, 2017.
875 Xie, S.-P., Kosaka, Y., and Okumura, Y. M. : Distinct energy budgets for anthropogenic and
876 natural changes during global warming hiatus, Nature geoscience, 9, 29-33,
877 doi:10.1038/ngeo2581, 2016.
878 Yang, D., Goodison, B. E., Metcalfe, J. R., Golubev, V. S., Bates, R., Pangburn, T., and Hanson,
879 C. L.: Accuracy of NWS 8'' standard nonrecording precipitation gauge: Results and
880 application of WMO intercomparison. J. Atmos. Oceanic Technol., 15, 54–68, 1998.
881 Zaveri, R. A. and Peters, L. K.: A new lumped structure photochemical mechanism for large-scale
882 applications, J. Geophys. Res., 104, 30387–30415, 1999.
883 Zaveri, R. A., Easter, R. C., Fast, J. D., and Peters, L. K.: Model for Simulating Aerosol
884 Interactions and Chemistry (MOSAIC), J. Geophys. Res., 113, D13204,
885 doi:10.1029/2007JD008782, 2008.
886 Zhao, C., Liu, X., Leung, L. R., Johnson, B., McFarlane, S. A., Gustafson Jr., W. I., Fast, J. D.,
887 and Easter, R.: The spatial distribution of mineral dust and its shortwave radiative forcing

888 over North Africa: modeling sensitivities to dust emissions and aerosol size treatments,
889 Atmos. Chem. Phys., 10, 8821–8838, doi:10.5194/acp-10-8821-2010, 2010.
890 Zhao, C., Liu, X., Ruby Leung, L., and Hagos, S.: Radiative impact of mineral dust on monsoon
891 precipitation variability over West Africa, Atmos. Chem. Phys., 11, 1879–1893,
892 doi:10.5194/acp11-1879-2011, 2011.
893 Zhao, C., Leung, L. R., Easter, R., Hand, J., and Avise, J.: Characterization of speciated aerosol
894 direct radiative forcing over California, J. Geophys. Res., 118, 2372–2388,
895 doi:10.1029/2012JD018364, 2013a.
896 Zhao, C., Chen, S., Leung, L. R., Qian, Y., Kok, J. F., Zaveri, R. A., and Huang, J.: Uncertainty in
897 modeling dust mass balance and radiative forcing from size parameterization, Atmos. Chem.
898 Phys., 13, 10733–10753, doi:10.5194/acp-13-10733-2013, 2013b.
899 Zhao, C., Hu, Z., Qian, Y., Ruby Leung, L., Huang, J., Huang, M., Jin, J., Flanner, M. G., Zhang,
900 R., Wang, H., Yan, H., Lu, Z., and Streets, D. G.: Simulating black carbon and dust and their
901 radiative forcing in seasonal snow: a case study over North China with field campaign
902 measurements, Atmos. Chem. Phys., 14, 11475-11491, doi:10.5194/acp-14-11475-2014,
903 2014.
904 Zhao, B., Liou, K.-N., Gu, Y., He, C., Lee, W.-L., Chang, X., Li, Q., Wang, S., Tseng, H.-L. R.,
905 Leung, L.-Y. R., and Hao, J.: Impact of buildings on surface solar radiation over urban
906 Beijing, Atmos. Chem. Phys., 16, 5841-5852, https://doi.org/10.5194/acp-16-5841-2016,
907 2016.

## List of Table

Table 1. Model configuration

| Atmospheric Process | WRF-Chem option |
|---|---|
| Microphysics | Morrison double-moment |
| Radiation | RRTMG for both shortwave and longwave |
| Land surface | CLM4 with SNICAR included |
| Planetary boundary layer (PBL) | YSU |
| Cumulus | No cumulus scheme used |
| Chemical driver | CBM-Z |
| Aerosol driver | MOSAIC 4-bin |
| Anthropogenic emission | NEI05 |
| Biogenic emission | MEGAN |
| Biomass burning emission | GFEDV2.1 |
| Dust emission | DUSTRAN |
| Meteorological initial and boundary conditions | ERA-Interim |
| Chemical initial and boundary conditions | MOZART-4 divided by 2 |

Table 2. Experiment design for various aerosol sources.

| Experiment | Anthropogenic Aerosols | Dust Aerosol | Transport | Description |
|---|---|---|---|---|
| CTRL | Y | Y | Y | Control experiment with all aerosol emissions/transports included |
| NoLocDust | Y | N | Y | Local dust aerosol emission is not included |
| NoLocAnth | N | Y | Y | Local anthropogenic aerosol emissions are not included |
| NoTran | Y | Y | N | Aerosols transported from outside the model domain are not included |
| CLEAN | N | N | N | Aerosol emissions/transports are not included |

Table 3. Experiment design for various aerosol pathways, using the CTRL aerosol emissions.

| Experiment | ARI | ACI | ASI | Description |
|---|---|---|---|---|
| NARI | N | Y | Y | ARI is not included |
| NASI | Y | Y | N | ASI is not included |
| NARS | N | Y | N | ARI and ASI are not included |

915 Table 4. Changes in surface temperature (K) and precipitation, SWE, and surface runoff in
916 percentage averaged over October 2012 to June 2013 due to overall and various aerosol effects for
917 the whole domain (34-42 °N, 117-124 °W, not including ocean points), mountain tops (with
918 elevation ≥ 2.5 km), and lower elevations ( < 2.5 km). Total impacts for the simulations from
919 October 2013 to June 2014 are also included as "Total_13-14".

| Region | Source/ pathway | T2 (K) | Precipitation (%) | SWE (%) | Surface runoff (%) |
|---|---|---|---|---|---|
| Whole Domain | Total | –0.19 | –6.87 | –3.17 | –6.58 |
| | Total_13-14 | –0.21 | –5.99 | –8.88 | –5.13 |
| | ARI | –0.14 | –0.47 | 1.88 | –0.21 |
| | ASI | 0.01 | –0.03 | –1.96 | 0.04 |
| | ACI | –0.06 | –6.26 | –2.67 | –6.30 |
| | LocAnth | –0.02 | –1.02 | –0.91 | –0.94 |
| | LocDust | 0.00 | –0.19 | –1.35 | 0.01 |
| | Tran | –0.17 | –2.97 | 1.89 | –2.90 |
| Mountain Tops | Total | 0.22 | –11.53 | –10.50 | –9.58 |
| | Total_13-14 | 0.15 | –9.90 | –15.57 | –3.55 |
| | ARI | –0.09 | –0.61 | 0.76 | –0.49 |
| | ASI | 0.12 | 0.26 | –3.94 | 1.10 |
| | ACI | 0.17 | –11.03 | –7.57 | –10.25 |
| | LocAnth | 0.03 | –1.75 | –1.60 | –2.06 |
| | LocDust | 0.10 | 0.31 | –2.99 | 1.49 |
| | Tran | –0.02 | –5.25 | –2.43 | –4.76 |
| Lower Elevations | Total | –0.21 | –6.62 | 0.42 | –6.42 |
| | Total_13-14 | –0.22 | –5.75 | 2.66 | –5.26 |
| | ARI | –0.14 | –0.46 | 2.43 | –0.19 |
| | ASI | 0.00 | –0.04 | –0.99 | –0.01 |
| | ACI | –0.07 | –6.00 | –0.27 | –6.09 |
| | LocAnth | –0.03 | –0.98 | –0.57 | –0.89 |
| | LocDust | 0.00 | –0.22 | –0.55 | –0.07 |
| | Tran | –0.17 | –2.85 | 4.01 | –2.81 |

920

**List of Figures**

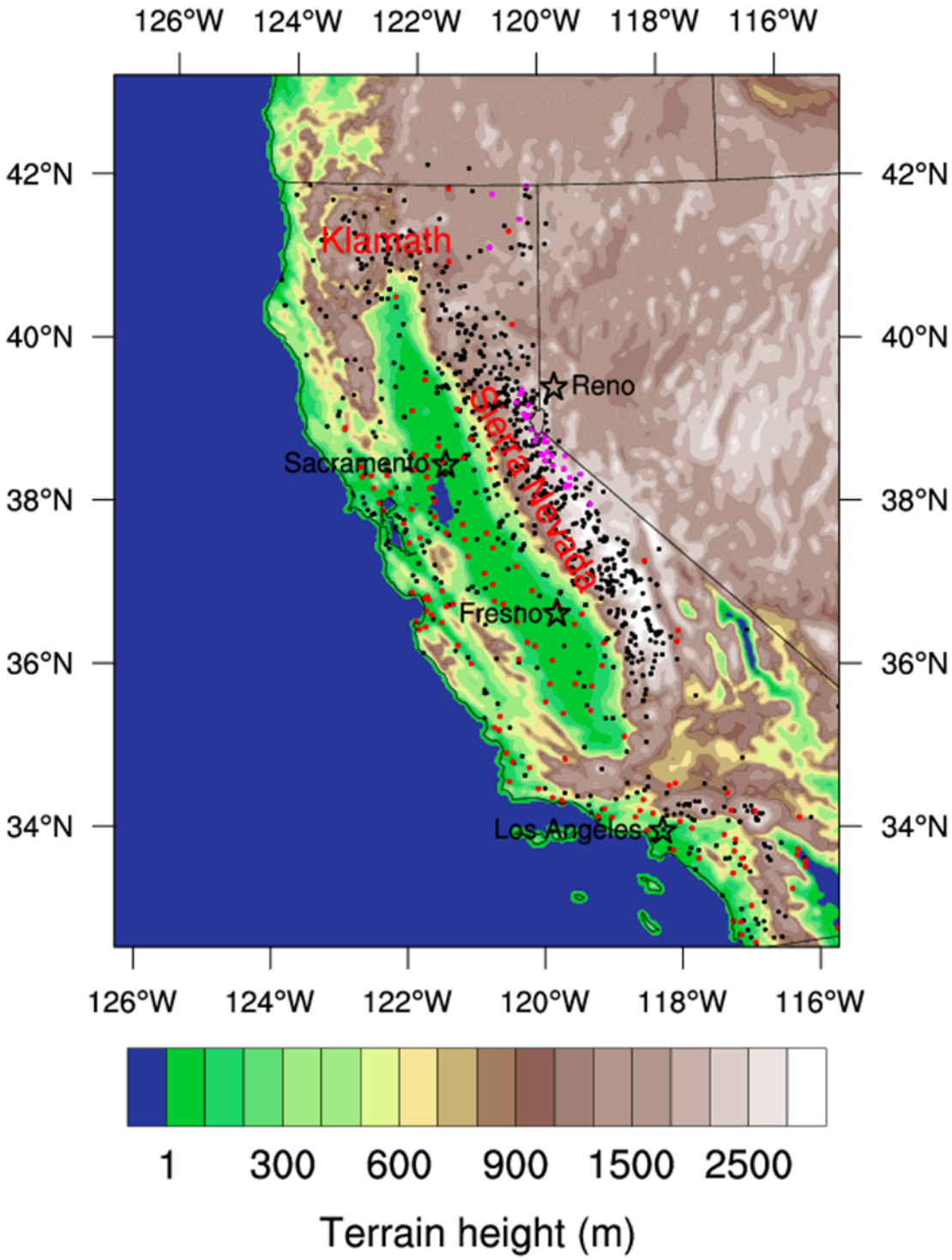


Figure 1. Model domain and terrain height (m). 991 DWR sites are represented by black dots; 138 CIMIS stations are represented by red dots; 32 SNOTEL sites are represented by magenta dots.

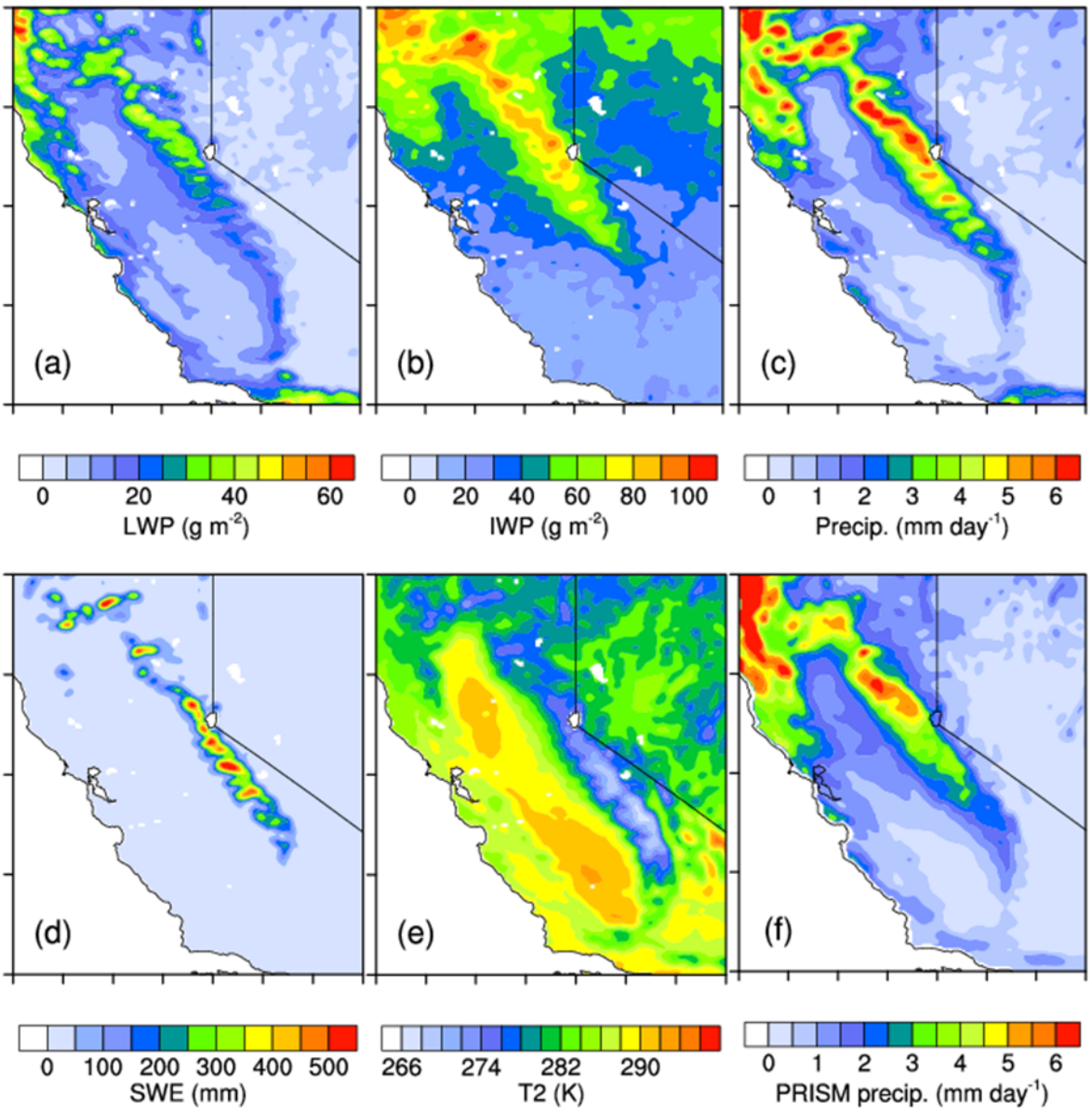


925

926 Figure 2. Model simulated (a) LWP (g $m^{-2}$), (b) IWP (g $m^{-2}$), (c) precipitation (mm $day^{-1}$), (d) SWE

927 (mm), and (e) temperature at 2 meters, T2 (K) from the CTRL simulation, and (f) PRISM observed

928 precipitation (mm $day^{-1}$), averaged over October 2012 to June 2013.

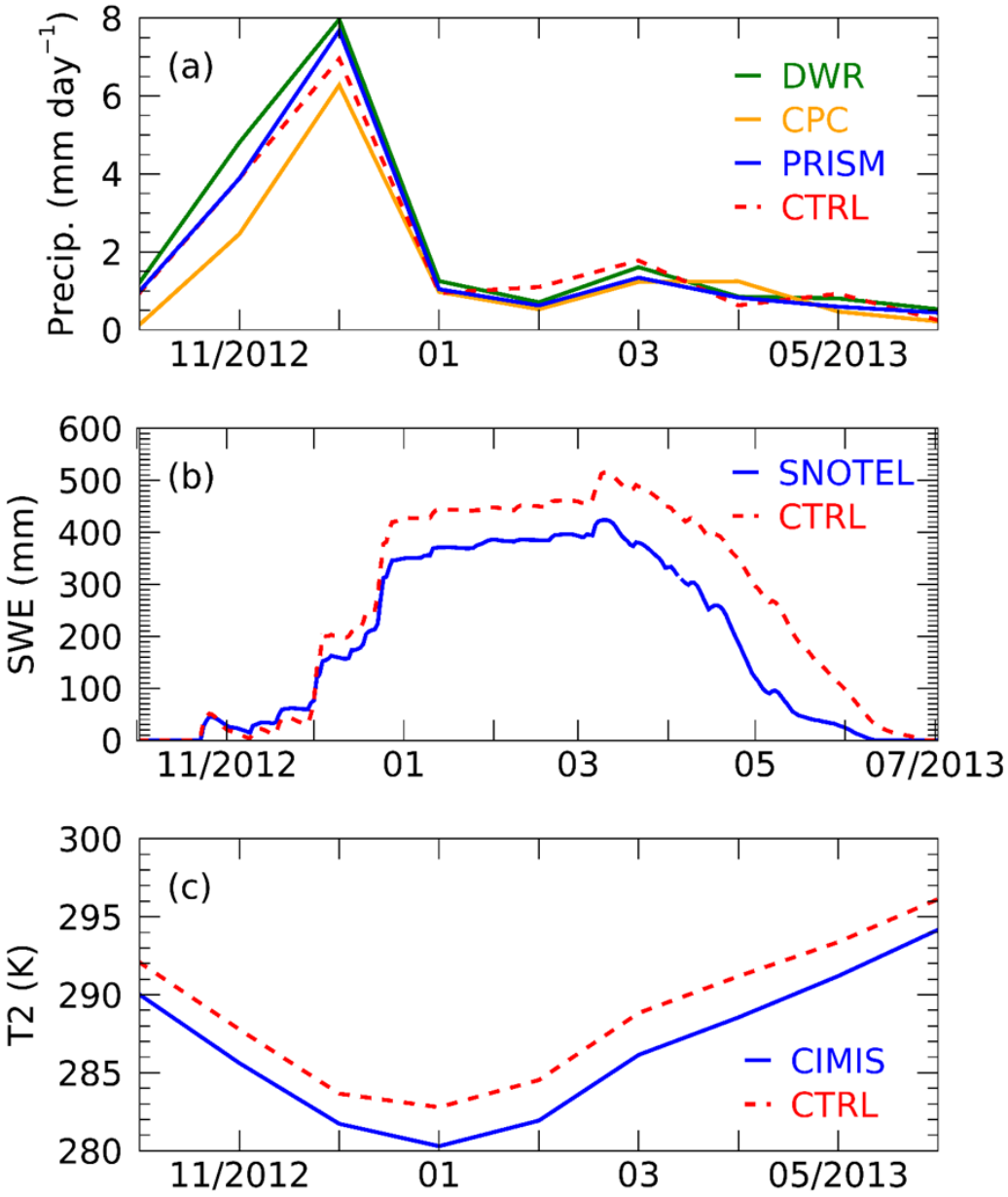


929

930 Figure 3. (a) Monthly mean precipitation (mm day$^{-1}$) from the CTRL simulation (red dashed) and
931 PRISM (blue), CPC (orange) and DWR (green) observations; (b) Daily accumulated SWE (mm)
932 from the CTRL simulation (red dashed) and SNOTEL observation (blue); and (c) Monthly mean
933 T2 (K) from the CTRL simulation (red) and CIMIS observation (blue). Model data are sampled
934 onto observational sites before the comparison is conducted.

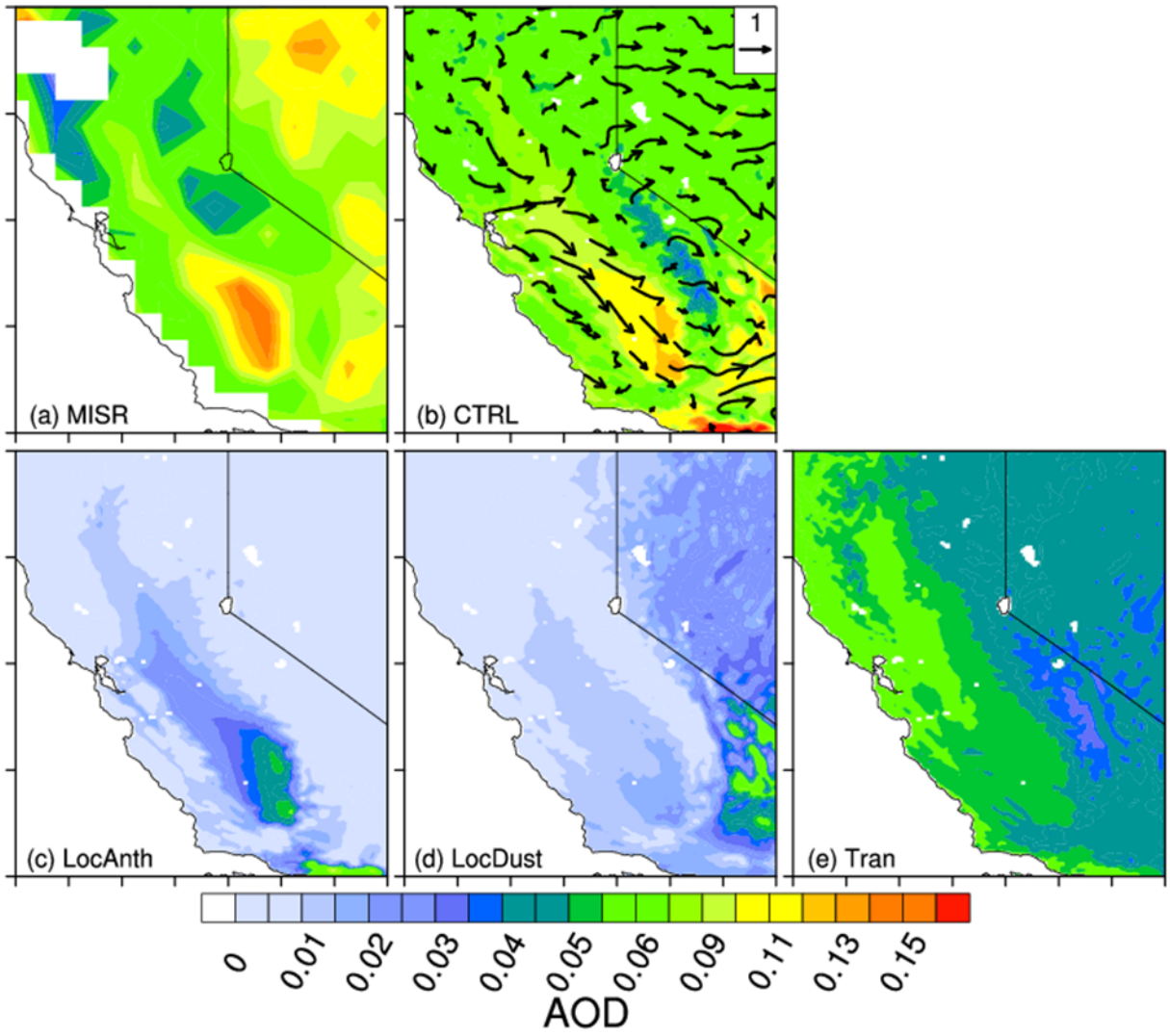


Figure 4. Spatial distribution of aerosol optical depth (AOD) averaged over October 2012 to June 2013 for (a) MISR observations, (b) all aerosols in the CTRL simulation, (c) local anthropogenic aerosols, (d) local dust aerosols, and (e) transported aerosols from outside the domain, derived from the difference between the CTRL simulation and the corresponding experiment (NoLocAnth, NoLocDust and NoTran), respectively. 10-m wind vectors from the CTRL simulation is shown in (b).

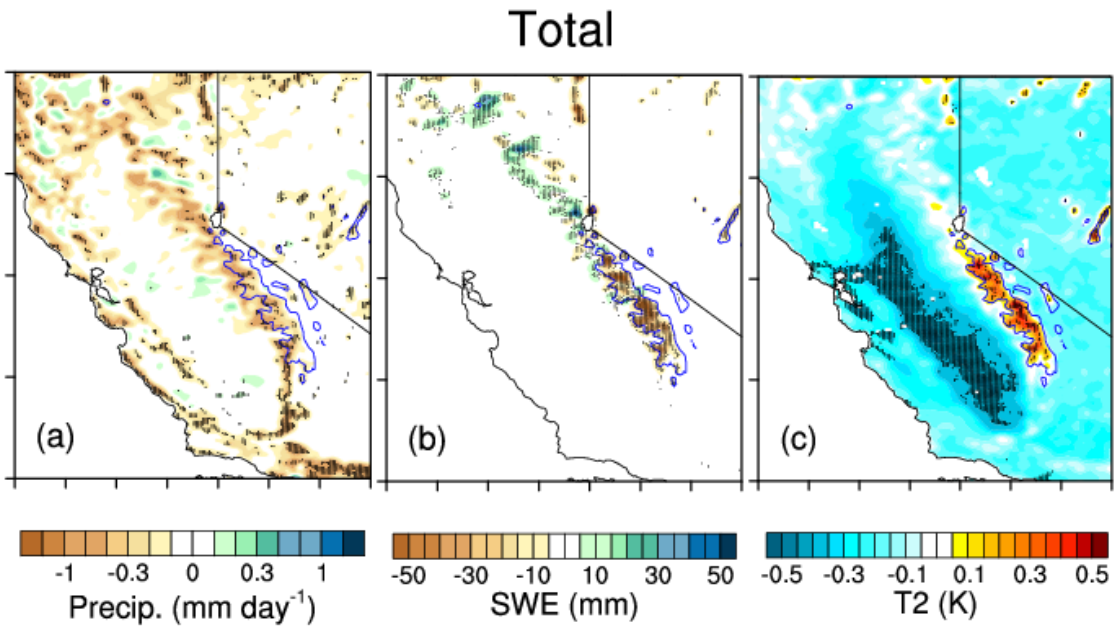


942

943 Figure 5. Total aerosol effects (CTRL – CLEAN) on spatial distribution of (a) precipitation (mm

944 day$^{-1}$), (b) SWE (mm), and (c) T2 (K). The dotted area denotes statistical significance above the

945 90% confidence level. Blue lines represent the mountain tops with elevation ≥ 2.5 km.

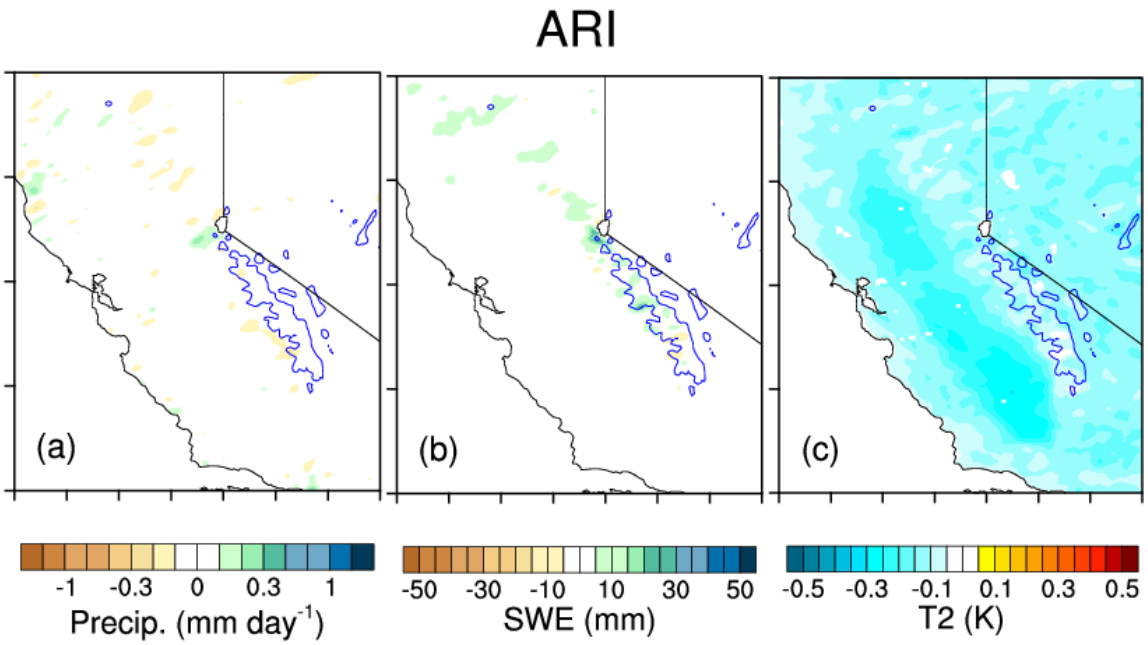


946

947 Figure 6. ARI effects (CTRL – NARI) on spatial distribution of (a) precipitation (mm $day^{-1}$), (b)

948 SWE (mm), and (c) T2 (K). Blue lines represent the mountain tops with elevation ≥ 2.5 km.

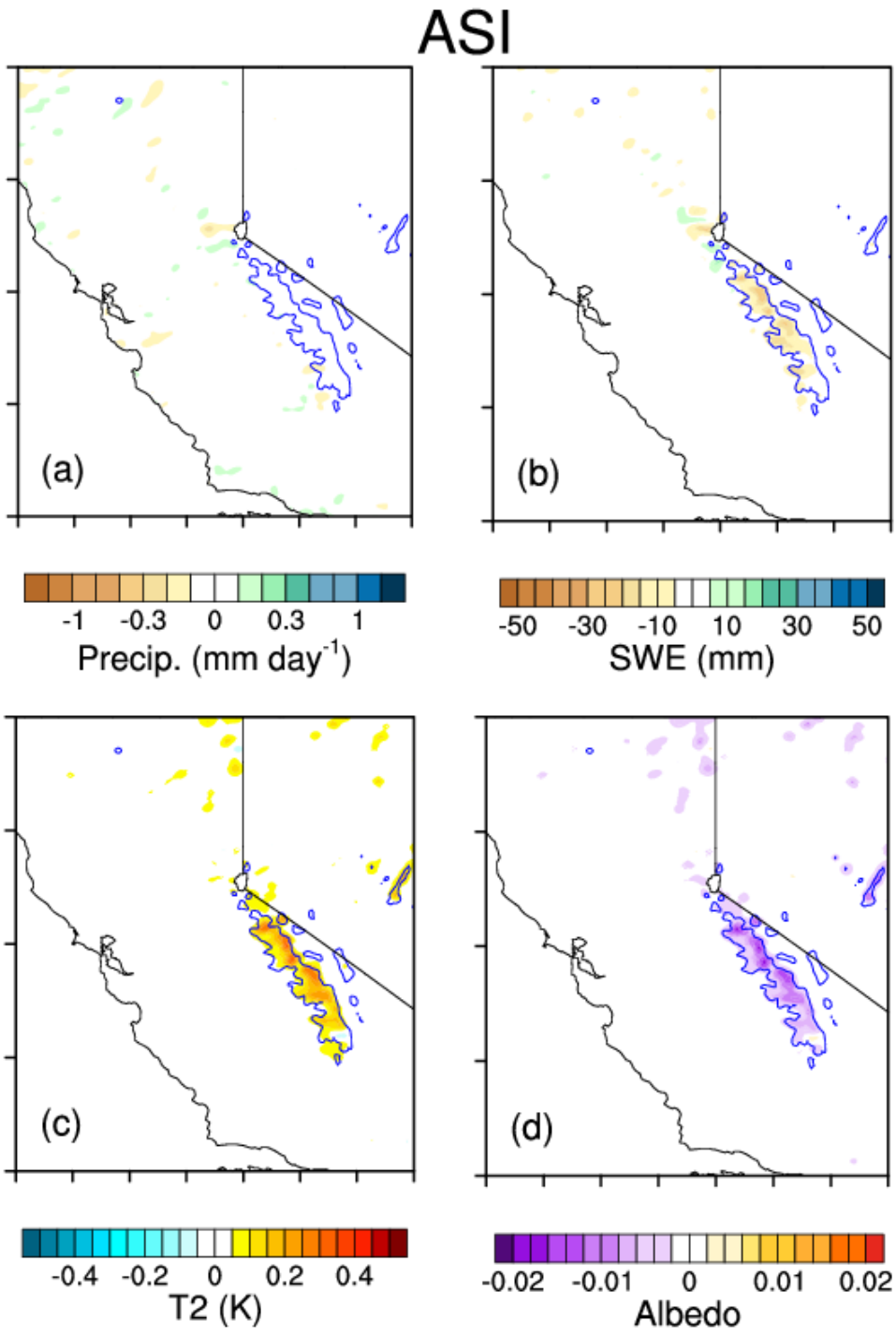


949

950 Figure 7. ASI effects (CTRL – NASI) on spatial distribution of (a) precipitation (mm $day^{-1}$), (b)

951 SWE (mm), (c) T2 (K), and (d) surface albedo. Blue lines represent the mountain tops with

952 elevation ≥ 2.5 km.

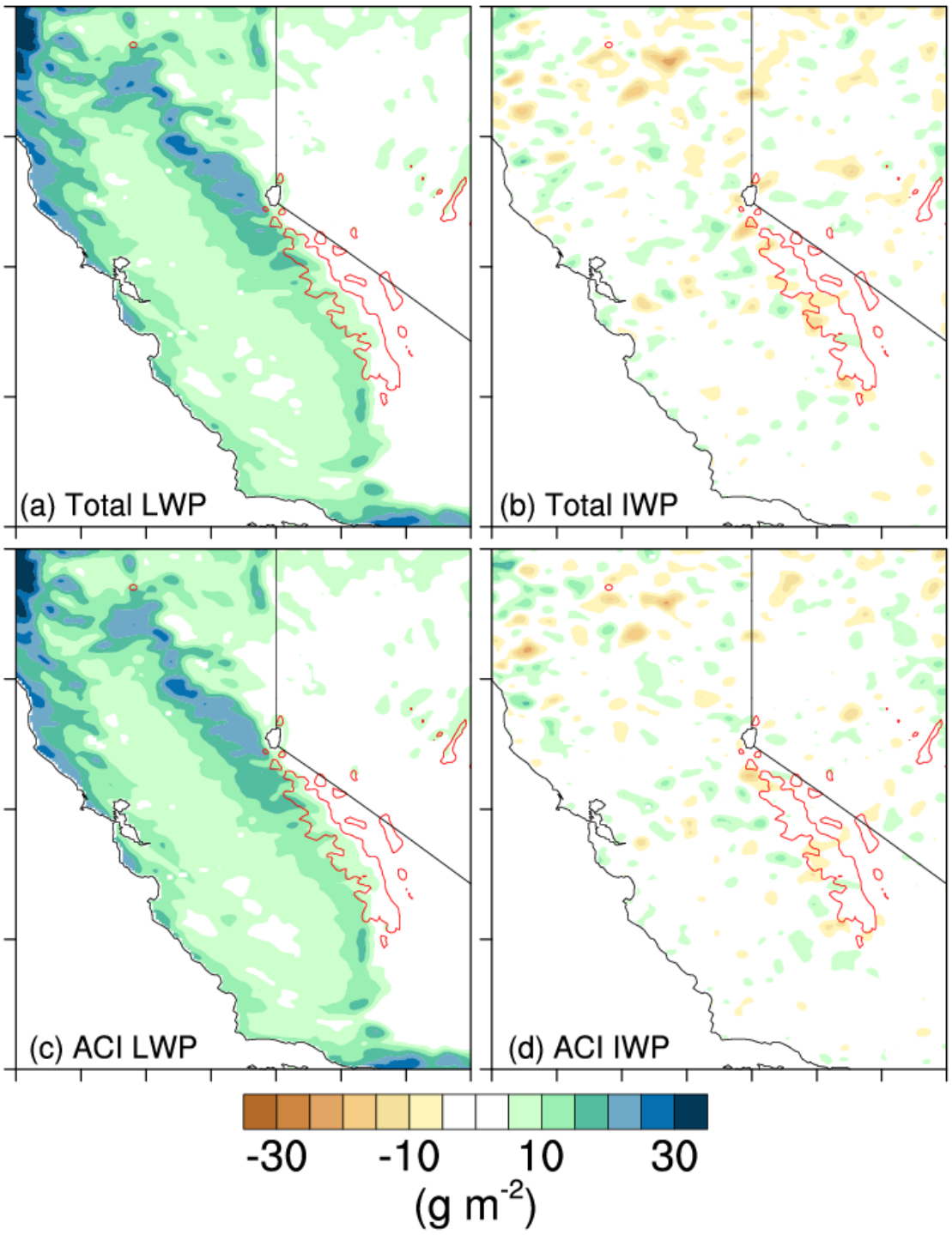


953

954 Figure 8. Differences in (a) LWP (g $m^{-2}$) and (b) IWP (g $m^{-2}$) due to all aerosol effects (CTRL –

955 CLEAN), and (c) LWP (g $m^{-2}$) and (d) IWP (g $m^{-2}$) due to ACI effect (NARS – CLEAN). Red

956 lines represent the mountain tops with elevation ≥ 2.5 km.

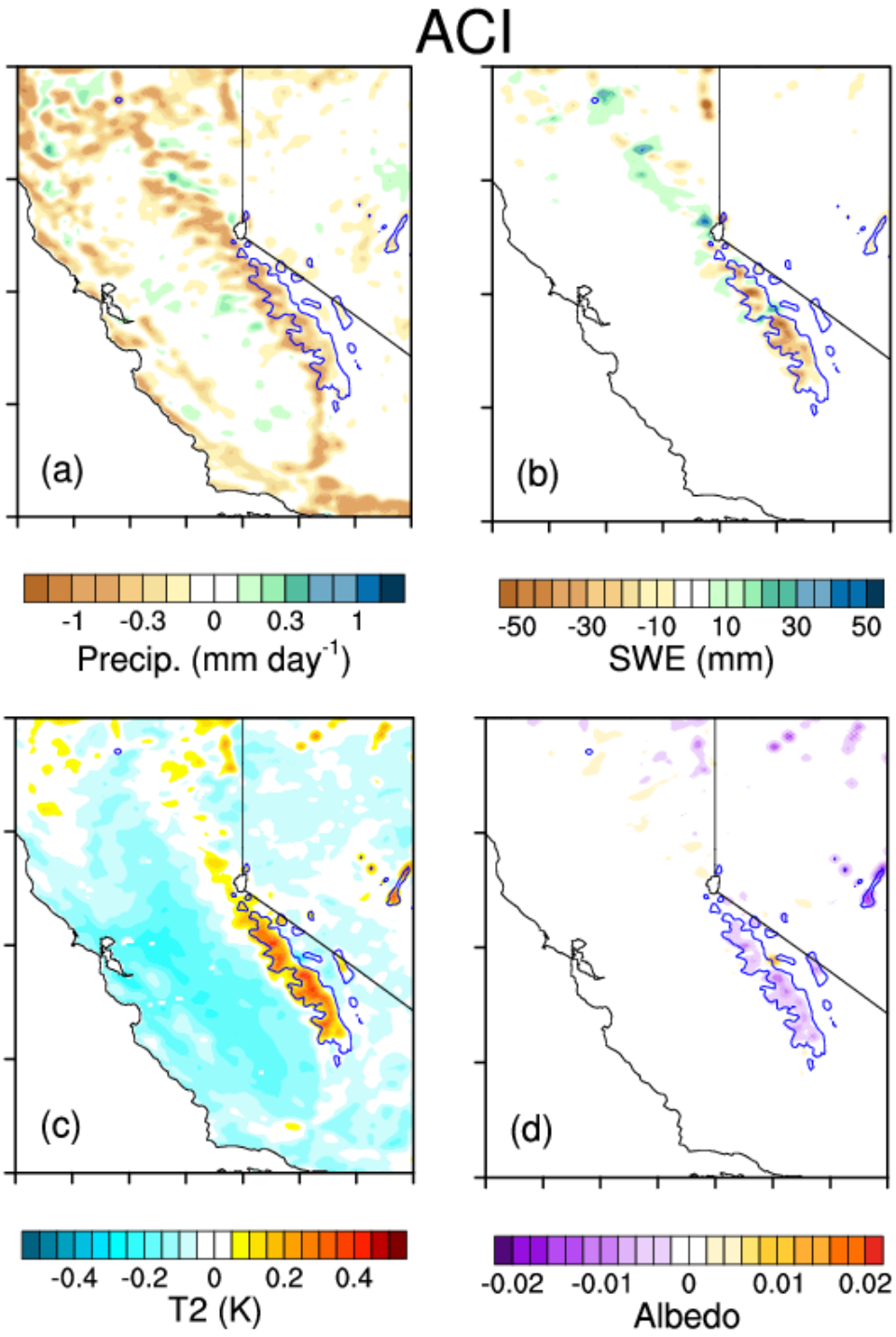


957

958 Figure 9. Same as Figure 7, but for ACI effect (NARS – CLEAN).

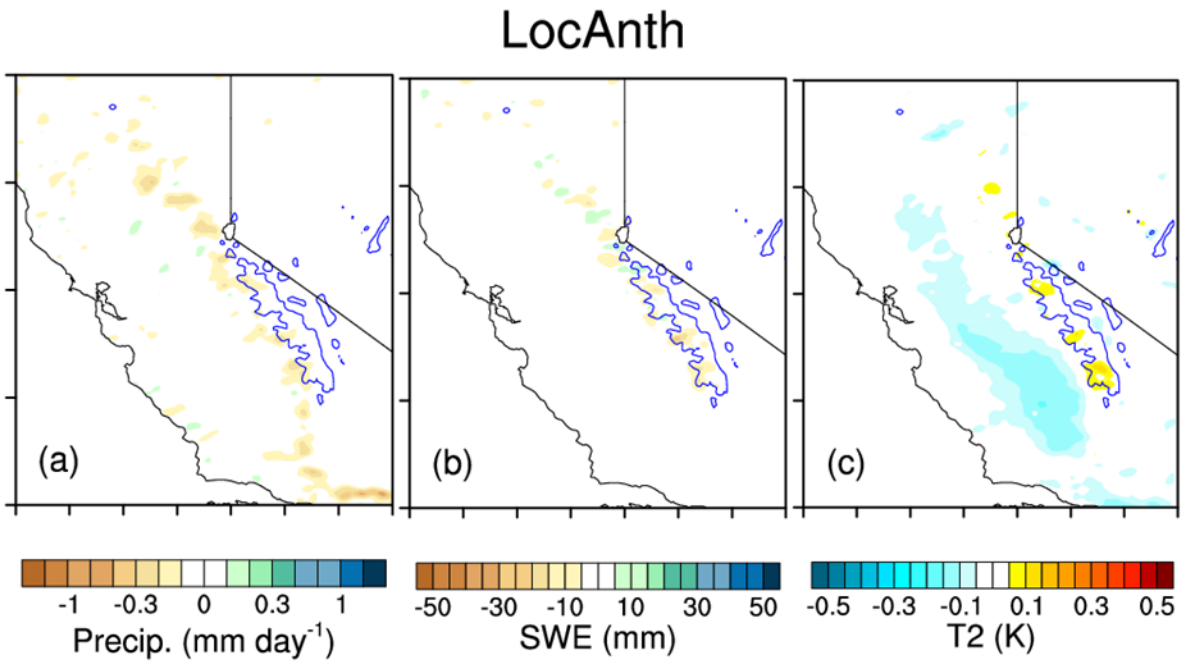


Figure 10. Effect of local anthropogenic aerosols (CTRL – NoLocAnth) on spatial distribution of (a) precipitation (mm day$^{-1}$), (b) SWE (mm), and (c) T2 (K). Blue lines represent the mountain tops with elevation ≥ 2.5 km.

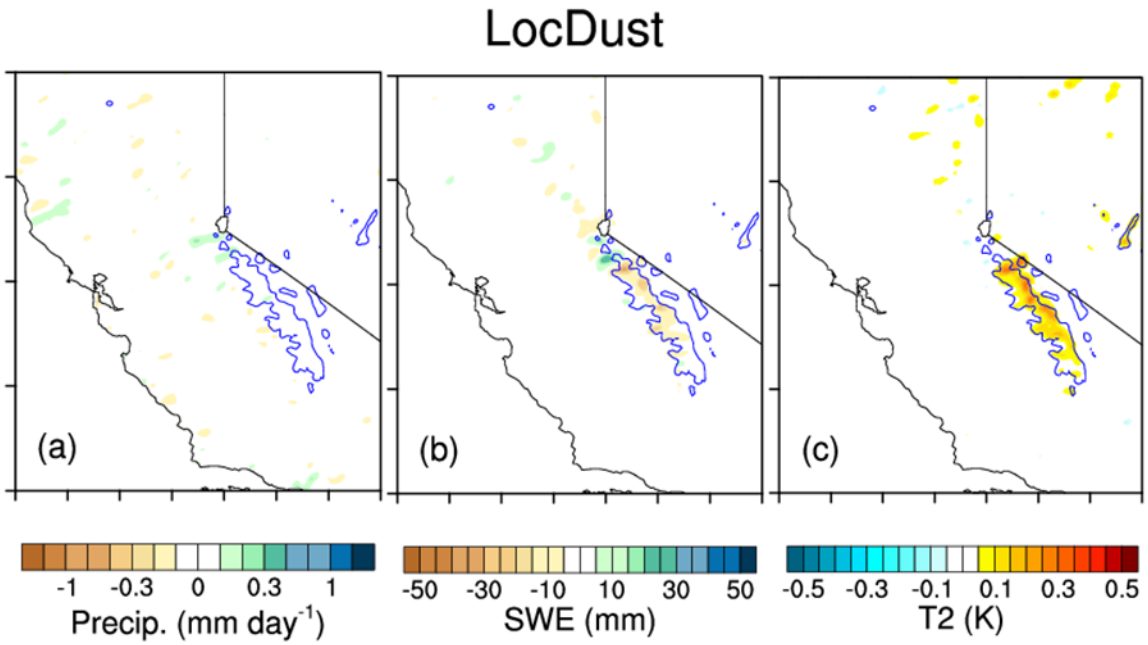


963

964 Figure 11. Same as Figure 10, but for the effect of local dust aerosols (CTRL – NoLocDust).

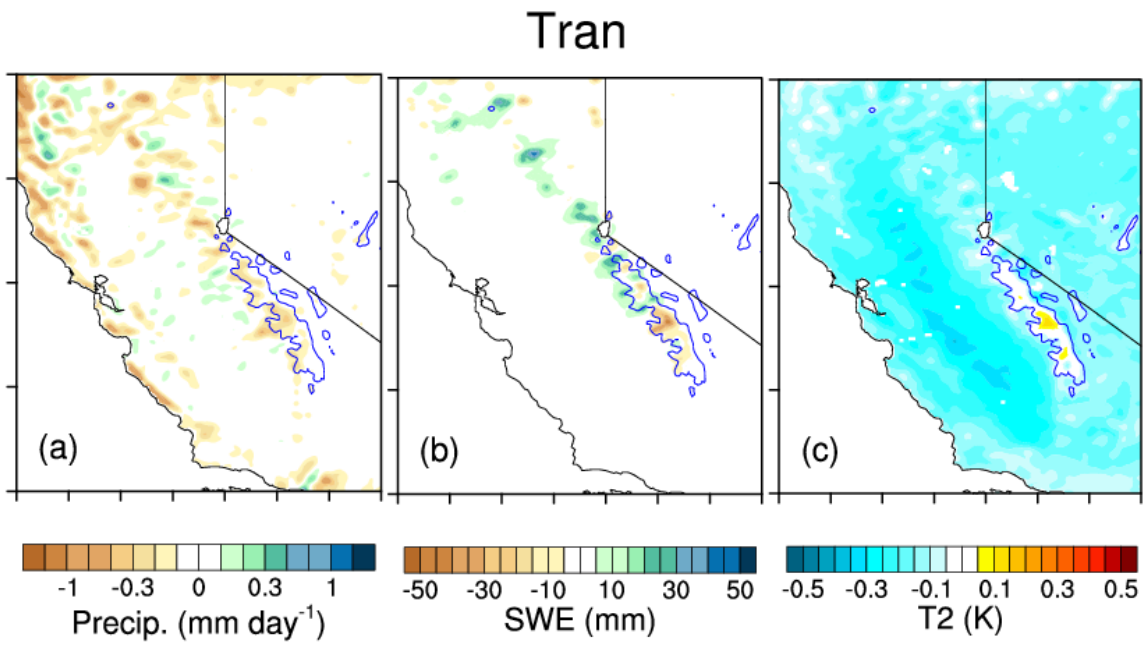


965

966 Figure 12. Same as Figure 10, but for the effect of transported aerosols (CTRL – NoTran).

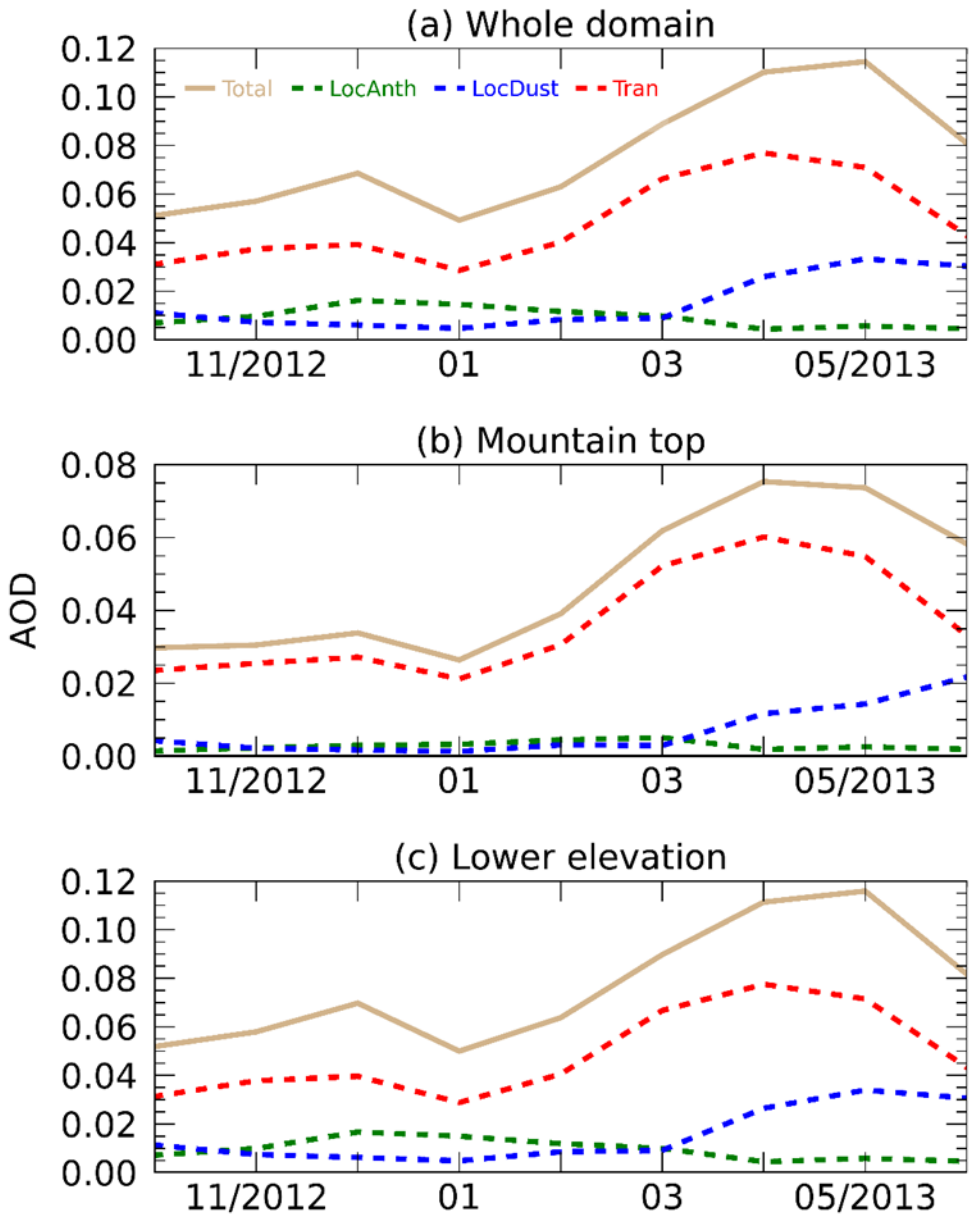


967

968 Figure 13. Monthly mean AOD simulated from CTRL for total aerosols (brown solid), local
969 anthropocentric aerosols (green dashed), local dust (blue dashed), and transported aerosols (red
970 dashed) averaged over (a) the whole domain (34-42 °N, 117-124 °W, not including ocean points),
971 (b) mountain tops (with elevation ≥ 2.5 km), and (c) lower elevation area ( < 2.5 km) from October
972 2012 to June 2013.

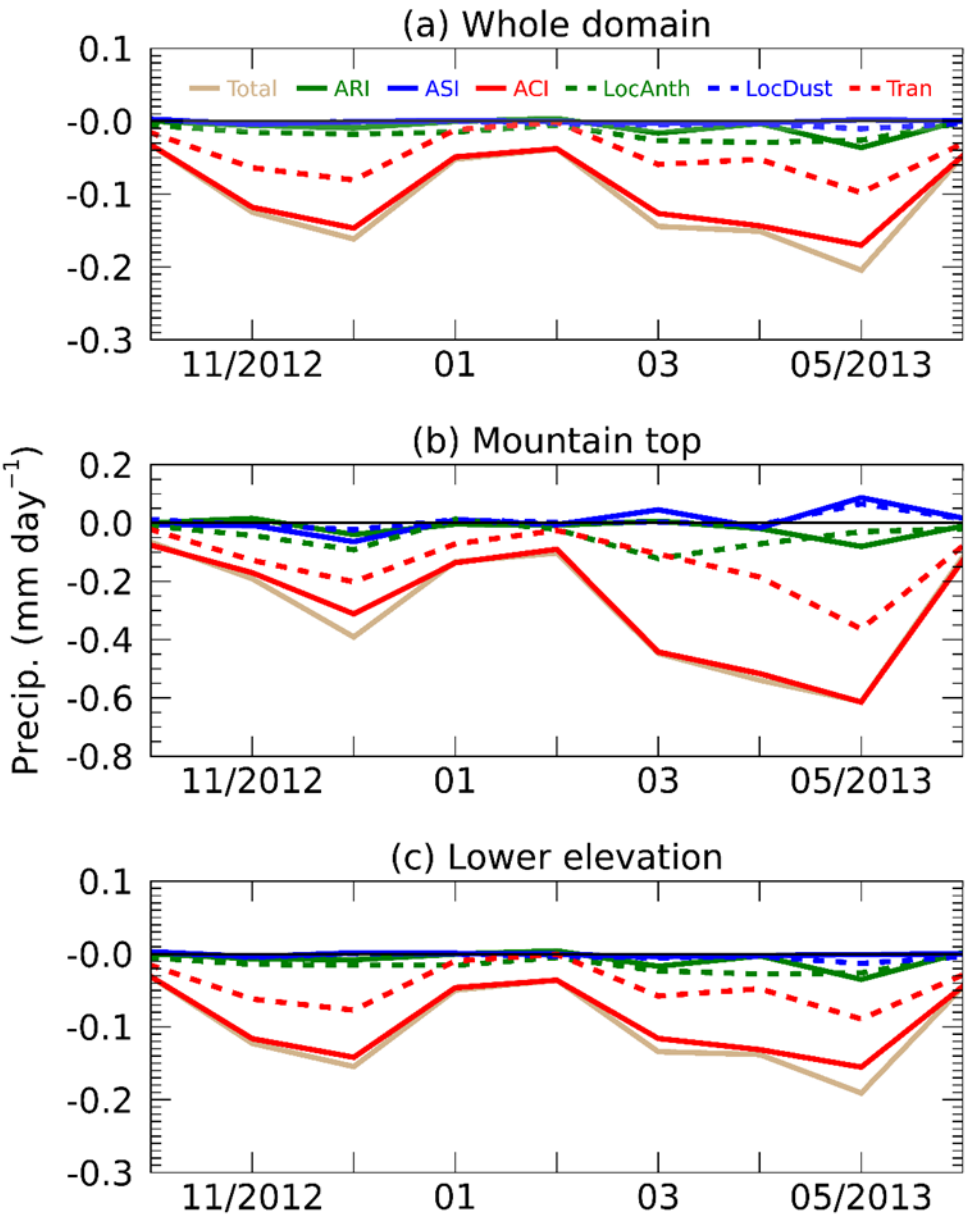


973

974 Figure 14. Monthly mean differences in precipitation (mm day$^{-1}$) due to total aerosols (brown
975 solid), ARI (green solid), ASI (blue solid), ACI (red solid), local anthropocentric aerosols (green
976 dashed), local dust (blue dashed), and transported aerosols (red dashed) averaged over (a) the
977 whole domain (34-42 °N, 117-124 °W, not including ocean points), (b) mountain tops (with
978 elevation ≥ 2.5 km), and (c) lower elevation area ( < 2.5 km) from October 2012 to June 2013.
979 Zero line is shown as thin black line.

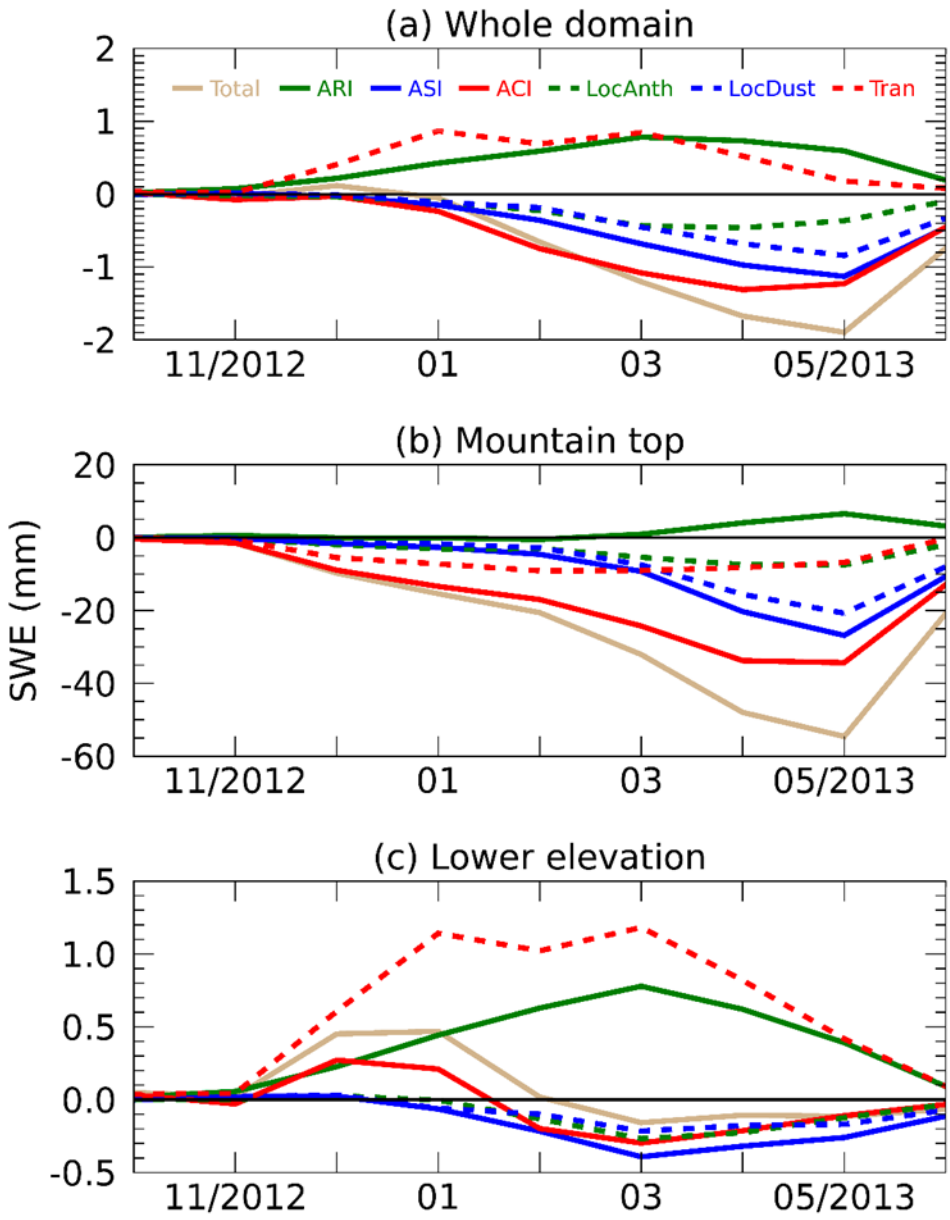


980

981 Figure 15. Same as Figure 14, but for SWE (mm).

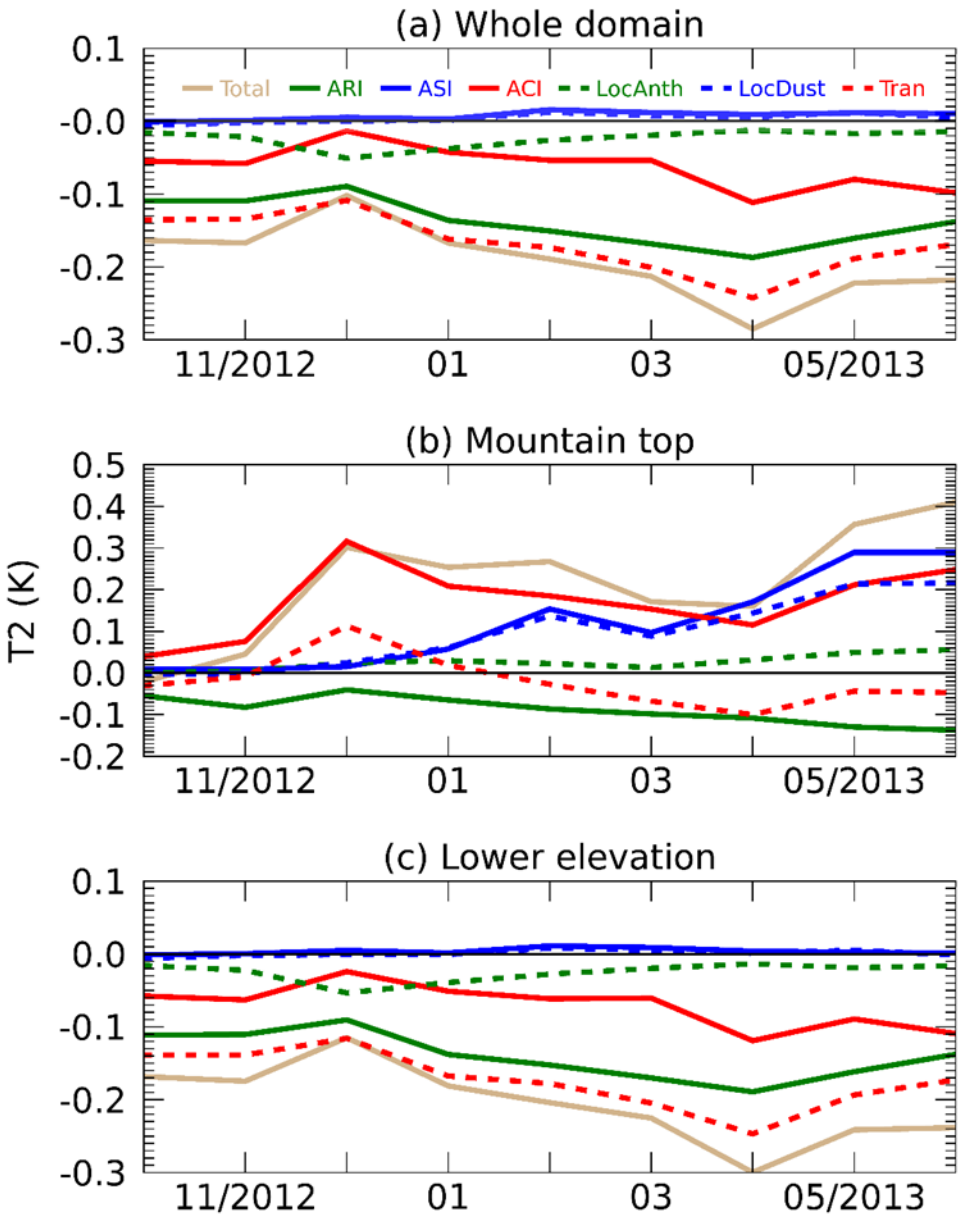


982

983 Figure 16. Same as Figure 14, but for T2 (K).

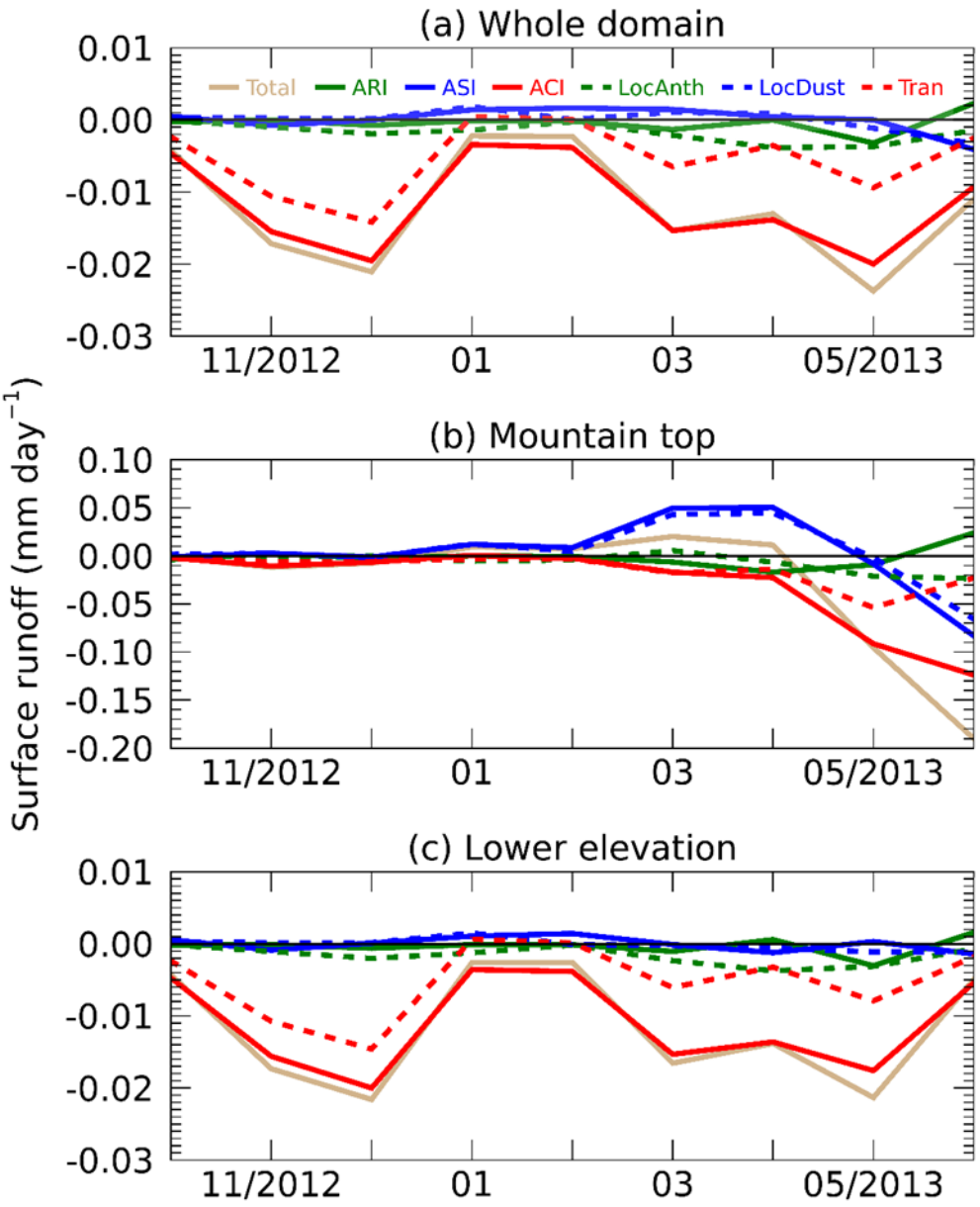


984

985 Figure 17. Same as Figure 14, but for surface runoff (mm day$^{-1}$).